Development of novel phospholipids-based ultrasound contrast agents intended for drug delivery and cancer theranostics

2016

Rodi Abdalkader

Content

Preface

Theranostics is a term that refers to the combination of therapy and diagnostics so that for example the same particle can both be used for finding a tumour and deliver drugs to treat it. Ultrasound (US) imaging is well-known and safe diagnostic tool that is widely used in many different applications. A limitation of US imaging is the difficulty in differentiating the blood vasculature from the surrounded tissues and therefore US contrast agents (UCAs) are often used for enhancing the contrast signal in the blood vasculature. UCAs are usually made of hydrophobic gases such as perfluorocarbons (PFCs) stabilized in bubble form by biocompatible shells. Recently, not only micro- and nanometer-sized gas bubbles but also liquid nanodroplets that can form gas bubbles *in vivo* (also called phase shift acoustic nanodroplets (PSANDs)) have been proposed. Gas cored UCAs usually have poor *in vivo* stability and by using liquid droplets instead that can be shifted into gas when it is needed, an attractive option can be introduced. After being used for diagnosis for many years, UCAs have recently also been used for enhancing the delivery of drugs and genes through the cavitation effects when combined with therapeutic US (TUS). However, most of the reported UCAs were investigated for imaging or for therapy separately. For theranostic applications, the balance between therapeutic and diagnostic characteristics will be critical. For instance, theranostic UCAs should give image enhancement and then often be simultaneously activated by TUS at the target site. This means they need high contrast signal and sufficient drug payload in one carrier and the stability has to be good enough for reaching the target but not too much good for the TUS activation. To solve this dilemma I have focused on three main aspects of perfluorocarbon carrier systems, first, the employment of phospholipids for stabilizing the UCAs, second the utilization of different hydrophobic

PFCs, and third, the development of suitable preparation method that is well designed for making theranostic UCAs. Phospholipids are biocompatible amphiphilic molecules that are the main component in cell membranes and have been frequently used in the biomedical research. Compared to other shell materials (e.g., polymers that form rigid shells), phospholipids can maintain better stability and resonant properties in UCAs due to their high flexibility and ability to adapt when an US wave leads to bubble oscillation. Moreover, drug and nucleic acids can be loaded into phospholipids shells easily by using the charge properties that lead to complex formation between drug molecules and the phospholipids' hydrophilic head groups. The other component, the PFCs are essential for US contrast signal enhancement. They have different physicochemical properties depending on structure and molecular weight that consequently affect UCAs size distribution, stability, and echogenicity. Moreover, the selection of proper preparation methods is also important. For example, sonication is a well-known method for preparing UCAs. However, it is not preferable in the case of thermo sensitive material and, thus, an alternative method such as mechanical agitation would be used.

In this thesis, I have developed several types of novel phospholipid-based UCAs. I aimed to show the merits and limits of each formulation and how we can improve these limits for better theranostic use. This included *in vitro* and *in vivo* evaluation of theranostic characteristics of these UCAs and based on that, the potential use of these carriers was then investigated for the purpose of gene delivery and cancer theranostics.

Chapter I

Formulation and evaluation of nano- and micro-sized phospholipids-based theranostic ultrasound contrast agents

Section I. 1

The development and characterization of mechanically formed bubbles

I.1.1 Introduction

Ultrasound contrast agents (UCAs) such as microbubbles (MBs) are spheres that are composed of gaseous cores and biocompatible shells. The size of MBs is usually 1-10 micrometres in diameter. Mostly low molecular weight perfluorocarbons (PFCs) are used as gaseous core due to their low solubility and diffusivity in water [1, 2]. Recently nano-sized bubbles (NBs) were also developed, with smaller diameter range between 400-600 nanometres [3, 4, 5]. In US imaging, UCAs are useful for enhancing the contrast signal in the blood vasculature and even more as a diagnostic tool for cancer and inflammatory diseases [6, 7]. Additionally, UCAs can efficiently enhance the delivery of nucleic acids through cavitation upon US irradiation [4, 8, 9].

UCAs have unique properties that can be useful in drug delivery. The biocompatible shell that is usually made of phospholipids, proteins, or polymers can be loaded with drugs and nucleic acids. On the other hand, the gaseous core provides this carrier with the resonant contrast signal (in the case of ultrasonography) and the cavitation that is needed for enhancing the delivery of the therapeutic payload.

The basic formulation of bubbles usually consists of two phases: the gas phase (bubbles) and the liquid phase (water or buffer) in which the bubbles are dispersed. To stabilise the bubbles, usually surface active molecules such as lipids are employed to form the border between gas and water, lower the surface tension, and also serve as a barrier that reduces the transport of gas molecules into the water phase. Bubbles are made by dispersing the gas with agitation forces through several methods such as:

sonication, shaking, homogenization, microfluidic mixing and coaxial electrohydrodynamic atomisation (CEHDA). However, these methods have some drawbacks related to the size distribution and stability of the produced bubbles. For example, sonication is a very common method but it often produces bubbles with a broad size distribution. Which should limit their clinical use due to some risk factors such as the blockage of vasculatures (embolism). Also, temperature increase might occur during the sonication process. In the case of microfluidic and CEHDA methods, although bubbles can be prepared with a narrow size distribution, still the multi-step procedures and high cost are limiting their use [10]. Therefore, introducing an alternative method for producing stable and homogenous bubbles is of importance. For that, I aimed in this study to evaluate the potential of a mechanical agitation method for producing homogenous and stable bubbles. Mechanical agitation is a simple and cheap method for mixing the liquid phase and the gas phase. In this protocol, no significant temperature elevation is generated and that can be useful when thermo-sensitive therapeutic agents are used. Based on that I hypothesised that by using such a method, homogenous bubbles can be obtained and therefore these bubbles should serve my theranostic purposes.

In this study, I succeeded to prepare nano-sized bubbles (MFBs) by using only mechanical agitation. The stability of MFBs was evaluated and then, several formulation factors such as lipid concentration, gas type and the storage conditions were tested for better theranostic use.

I.1.2. Materials and methods

I.1.2.1. Phospholipids

1, 2 distearoyl-sn-glycero-3-phosphocholine (DSPC) was purchased from Avanti Polar Lipid Inc. (Alabaster, AL, USA) and 1, 2 distearoyl-sn-glycero-3-phosphoethanolamine -N-[amino-(polyethylene glycol)-2000] (PEG-$_{2000}$-DSPE) was purchased from NOF Co. (Tokyo, Japan).

I.1.2.2. MFBs preparation

DSPC and PEG$_{2000}$-DSPE in 94:6 molar ratio were dissolved in chloroform, followed by evaporation of the chloroform in a rotary evaporator at 25°C for 30 min; this was followed by further drying under vacuum at room temperature overnight. Lipid film was hydrated with phosphate buffer solution (PBS) at 65 °C for 60 min under mild agitation. The final lipid concentration after hydration was adjusted to 8 mg/ml. The sample was then exposed to bath sonication for 10 min followed by tip sonication for 3 min giving a fine lipid dispersion with diameters ~100 nm (liposomes). For preparing MFBs, liposomes were diluted with PBS in sterilised vials to obtain final lipid concentrations of (0.25-0.5-1) mg/ml. The air in the vial was taken by a syringe and after capping 12 ml of perfluoropropane (PFP) or perfluorobutane (PFB) (Takachiho Chemical Industries Co., Tokyo, Japan) was injected. The pressure inside the vial was estimated to be ~2 atm using the general law of gases:

$$PV = nRT \quad (1)$$

Where P is the pressure, V is the volume, n is the number of moles, R is the universal gas constant, and T is the temperature in Kelvin. At a fixed temperature, R and T were considered constant and the pressure was then calculated through the change of gas volume:

$$P_{start} \times V_{start} = P_{end} \times V_{end} \quad (2)$$

To obtain the MFBs, a shaking machine (Ultra Mate 2, Victoria, Australia) was used for 60 s.

I.1.2.3. Characteristics of MFBs

The particle size and zeta potential of the liposomes and MFBs were determined using a Zetasizer Nano ZS instrument (Malvern Instruments Ltd., Worcestershire, UK). For the optical imaging, diluted MFBs were mounted on a 35 mm glass slide covered with a cover glass and images were obtained using light microscopy. Surface area of bubble was calculated from the equation:

$$SA\ (bubble)\ = 4\pi r^2 \qquad (3)$$

Where SA is the surface area of one bubble; and r is the bubble radius. Numbers of lipids molecules per one bubble were estimated by the following equation:

$$N = \frac{SA\ (bubble)}{SA\ (lipid)} \qquad (4)$$

Where N is number of lipids per one bubble; SA (lipid) is the lipid surface area and in case of several lipid compositions (SA (lipid) = SA (lipid) $_1$×Mol fraction (lipid) $_1$+ $_{SA}$ (lipid) $_2$×Mol fraction (lipid) $_2$+ $_{SA}$ (lipid) $_n$× Mol fraction (lipid) $_n$)

I.1.2.4. Gas content

PFP content was measureed similarly as reported previously [11]. In short, after preparing MFBs, the vial was opened at room temperature and a sample of 25 µl of MFBs was taken. Collected samples were kept in special vials designed for gas chromatography and then vials were tightly caped. Samples were analysed by GC-MS (Shimadzu GCMS-QP2010 spectrometer with a HS-20 headspace sampler).

I.1.3. Results

The mechanical agitation using a shaking machine was applied for 60 sec. MFBs

were more stably formed with homogenous size distribution in the presence of perfluorocarbon gases such as PFP and PFB. In the presence of nitrogen gas, bubbles were hardly formed and soon after couples of measurements bubbles were dissolved and disappeared (Fig. 1). During agitation, a mild temperature elevation was recorded in the vials (from 22.2 ± 1.5 °C before agitation to 30.1 ± 2.7 °C after agitation). The effect of lipid concentration on MFB's formation and stability at room temperature (RT) was also tested. Freshly prepared MFBs with different lipid concentrations had relatively narrow size distribution after preparation with a slight increase in MFB's size when lipid concentration increased from 0.2 mg/ml to 0.5 mg/ml. This observation consisted with the increase of the MFB's surface area and the number of lipids molecules in each bubble. No more change was induced in MFB's size when lipid was further increased to 1 mg/ml. However, after 24 hr only MFBs that were made with final lipid concentration of 0.5 mg/ml still had a homogenous size. On the other hand, MFBs that had final lipid concentrations of 0.25 gm/ml and 1 mg/ml were almost disappeared and demonstrated in a very scattered size distribution (Fig. 2).

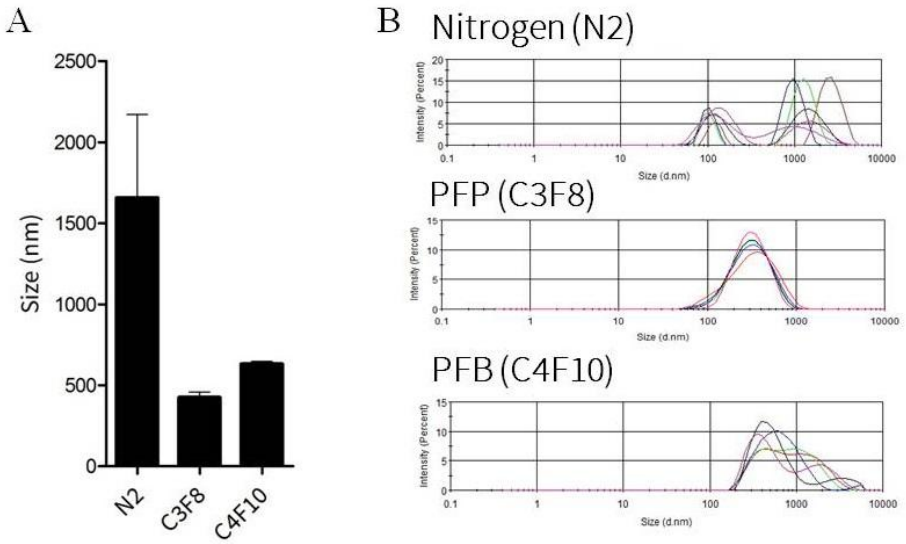

Fig.1. Size measurements of MFBs with different gases where C3F8 is perfluoropropane gas, C4F10 is perfluorobutane gas, and N2 is nitrogen gas. (A) Mean bubble size (n = 3; mean ± SEM). (B) Size

distribution histograms.

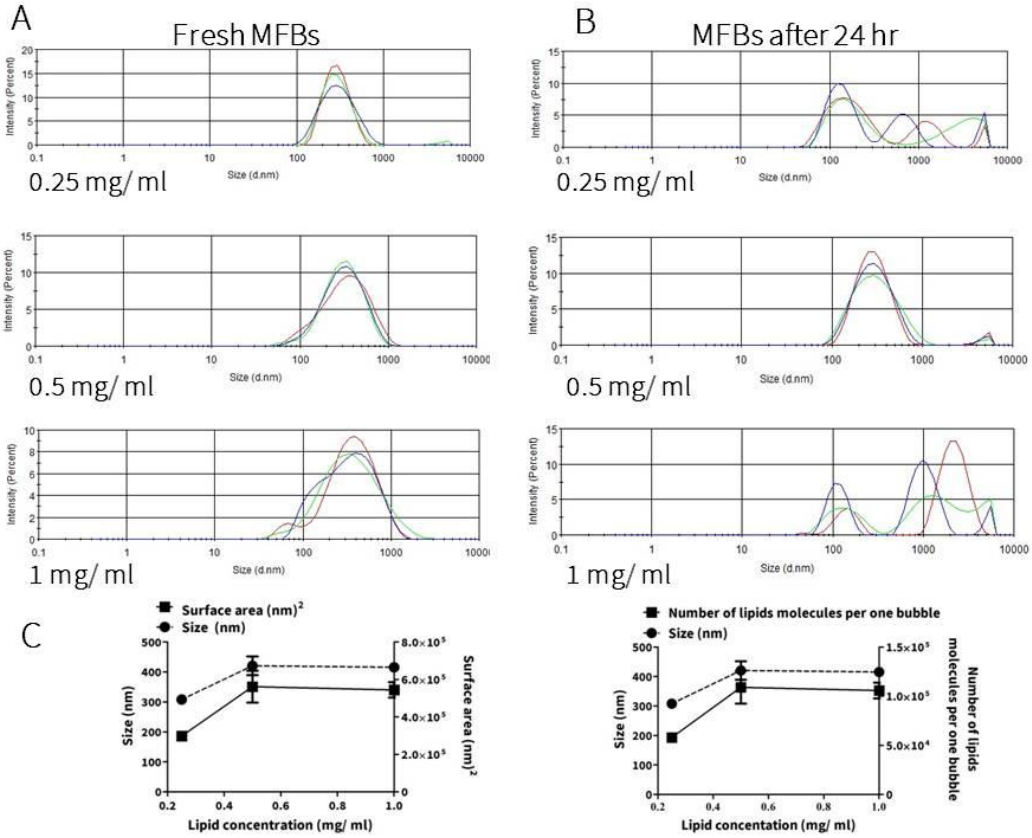

Fig. 2. The effects of lipid concentration on MFB's size distribution and stability in room temperature. (A) Size of freshly prepared MFBs (n =3). (B) MFBs after 24 hr storage at room temperature (n =3). (C) Bubbles size versus surface area and the number of lipids per one bubble.

The amount of PFP immediately after uncapping the vial was quantified to 54. 6± 8.4 µl per 1 mg of lipid (n = 3). MFB's stability in atmospheric pressure and at 4 °C was further investigated for a longer time. Size measurements immediately after vial uncapping were considered as 0 time. MFBs had homogenous and stable size at room temperature (RT) even after 24 hr at atmospheric pressure (n =10; for each time point) with a slight reduction in the size (Fig. 3).

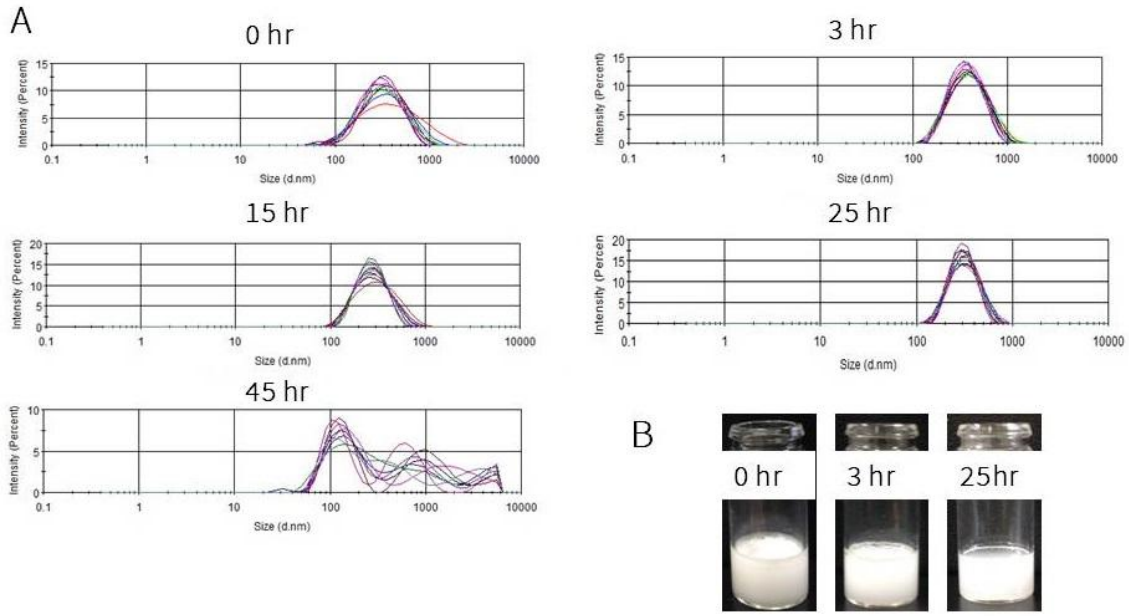

Fig. 3**.** Results of size measurements of MFBs made with PFP gas (C3F8) and left at the atmospheric pressure for different time points (A). MFB's size distribution histograms of ten measurements during 25 hr. (B). The visual appearance of MFBs at 0, 3, and 25 hr post exposing of MFBs to the atmospheric pressure conditions.

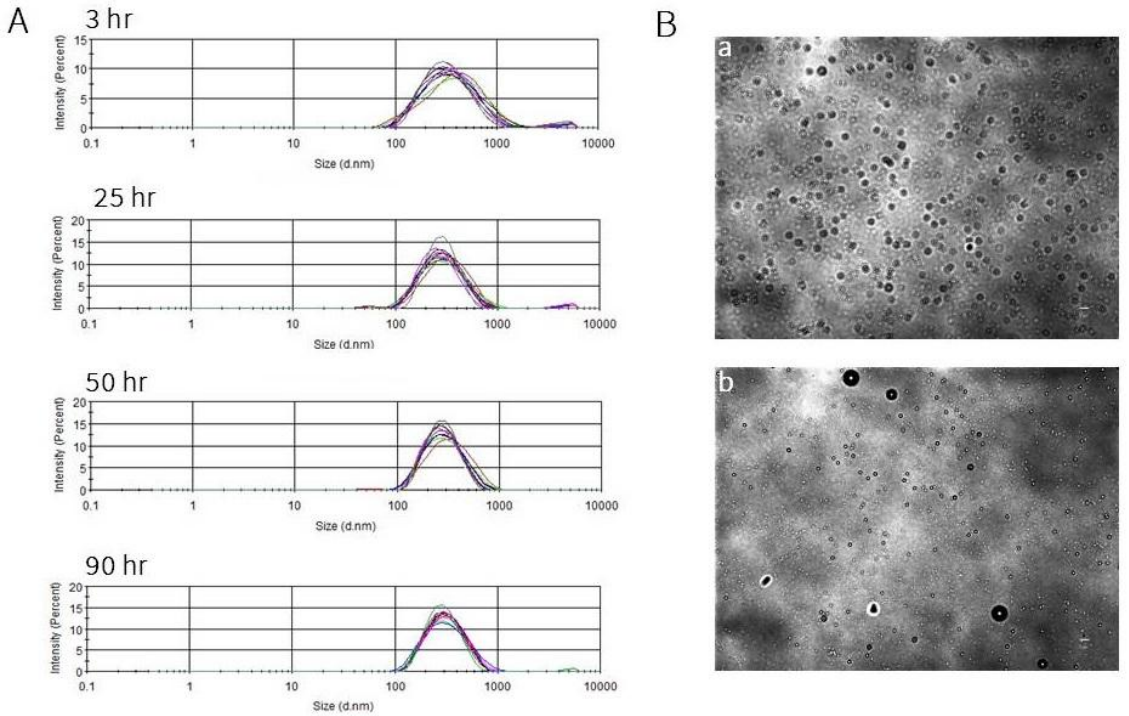

Fig. 4. MFB's size stability at 4 ° C. (A). Size distribution at different time points (n = 10) are shown. (B). Optical images of freshly prepared MFBs (a) and MFBs kept at 4ºC for 90 hr (b). (scale bar, 5 µm).

On the other hand, MFBs that kept at 4 ℃ tended to have better size distribution. The size was also slightly decreased after 3 hr but then sustained almost for 90 hr at 4 ℃ (Fig. 4 A). At this point, MFBs still existed and size peaks were homogenous. The optical images of preserved MFBs at 4 ℃ also supported these findings and bubbles still had a spherical shape and a sub-micron size even after 90 hr (Fig. 4 B/ b).

I.1.4. Discussion

Recently many works have been conducted for the purposes of preparing stable and homogeneous bubbles [10, 12]. However, most of these methods (e.g., sonication method and microfluidic method) are associated with some drawbacks including the instability of the generated bubbles and complexity of the fabrication process [12, 13]. In my results, only mild mechanical agitation for 60 s was enough for producing bubbles with a narrow size distribution. This method did not induce any significant elevations in temperature of the samples. This implies that the present method can be used with sensitive theranostic material toward high temperature or sonication power. For optimising the formulation conditions for the fabrication of mechanically formed bubbles, firstly the gas type was considered. Comparing with low molecular weight gases (e.g., nitrogen gas) perfluorocarbons (e.g., PFP and PFB) have low solubility and diffusivity, and thus bubbles can be formed with better size distribution and stability [14]. The amount of encapsulated PFP in MFBs was higher than the previously reported bubbles that were prepared by sonication method with a similar lipid composition [11]. Secondly, I have demonstrated that lipid concentration also has an impact on bubble formation and stability. It is believed that the increase in final lipid concentration enhanced the monolayer packing in MFBs by incorporating more lipid in the bubbles

shell as the number of lipids molecules per bubbles was increased. Enough amount of the lipid guarantees the decrease in surface tension and thereby results in more stable bubbles. Less lipid in the bubbles shells (at 0.25 mg/ml) apparently affected the stability and bubbles were rapaidly disappeared. Higher concentration of lipid (1 mg/ml) also tended to destabilise MFBs possibly due to the over packing in shells or single micelles formation that might adhere on the bubbles due to Oswald repining mechanism. My results are consistent with investigations by Shih and Lee, who reported that the lipid concentration tended to affect the bubble size and characteristics [13]. Garg et al., also showed that phospholipid monolayer in the bubble shells are packed more tightly than phospholipid bilayer leading to the increase of van der Waals interactions between phospholipid molecules and that reduce the gas leakage that destabilise bubbles [15]. I have used DSPC in MFBs to improve the stability of bubbles as it was reported that bubbles made of rigid phospholipids such as DSPC could decrease gas diffusion [16]. It was also reported that the coexistence of PEG-$_{2000}$-DSPE in a fraction more than 5 % with DSPC leads to more stable monolayer packing at the interface between water and air [17].

Aged MFBs storaged at 4 ºC were more stable than those at the RT. It was explained that the preservation condition at 4 ºC can increase the shell elasticity due to the decrease in activation energy that leads usually to the shell rupture. Although the previous report was conducted with bubbles made with protein shells, but not with phospholipids, it is still possible to consider that phospholipid shells have a similar behaviour [18].

These findings suggested that mechanical agitation can be used for the generation of bubbles with good stability. Furthermore, the stability of bubbles was enhanced

through the optimisation of gas type, lipid concentration, and preservation temperature. Therefore, this method has strong potential in the preparation of MFBs for future theranostic applications.

Section I. 2

The development of mechanically formed bubbles loaded with doxorubicin

I.2.1. Introduction

Doxorubicin (DOX) is one of the most used anti-cancer agents for a variety of solid tumours such as osteosarcoma, leukaemia, Hodgkin`s lymphoma, and breast cancer [19]. The combination of DOX and bubbles with TUS irradiation has been found to enhance DOX uptake in cells through sonoporation [20, 21]. Also, many reports have shown the possibility of loading DOX into bubbles by electrostatic interactions [22, 23].

However, most of these reports have focused on the therapeutic use of the formulations. The diagnostic potential has been less in focus. For cancer theranostic applications, both DOX and perfluorocarbons (PFCs) gas should be stably encapsulated in the same bubbles. Therefore obtaining such balance is crucial for better theranostic use.

In Section I 1, I showed that homogenous phospholipid-based bubbles could be produced by using a mechanical agitation method. Also, my results indicated that bubbles made especially with perfluopropane gas (PFP) had narrow size distribution and good stability for a long time. Moreover, it was reported that anionic phospholipid distearoylphosphatidyl glycerol (DSPG) incorporated in the bubbles could enhance their half-life both *in vitro* and *in vivo* [24]. At the same time, DSPG can offer a platform for DOX loading in bubbles shells mainly through electrostatic interactions. Taking all of these in consideration, I expected that DOX-loaded bubbles (DLBs) can be formed by using the previous method.

In this section, I optimised the conditions required for the preparation of stable

DLBs by using mechanical agitation. The balance between the encapsulation of DOX and PFP gas was studied. Also, the *in vitro* theranostic characteristics such as echogenicity and DLB's destructibility by TUS were tested as well.

I.2.2. Materials and methods

I.2.2.1. Phospholipids

DSPG, 1, 2-dipalmitoyl-sn-glycero-3- phosphatidylcholine (DPPC) and PEG_{2000}-DSPE were purchased from Avanti Polar Lipid Inc. (Alabaster, AL, USA) and NOF Co. (Tokyo, Japan).

I.2.2.2. DOX-liposome and DLBs preparation

DPPC, DSPG and PEG_{2000}-DSPE in a 70:25:5 molar ratio were dissolved in a MeOH: chloroform mixture, followed by evaporation of the solvents in a rotary evaporator at 25°C for 30 min. This was further dried under vacuum at room temperature overnight. Ten mg of lipid film was hydrated with 3 ml of 5% glucose solution (containing 2 mg of DOX) at 65 °C for 60 min under mild agitation, to obtain a lipid dispersion (liposomes). The final lipid concentration after hydration was adjusted to 3 mg/ml. For preparing bubbles, 0.5 ml of the lipid dispersion was added to a 5 ml sterilised vial. The air in the vial was replaced with PFP gas (Takachiho Chemical Industries Co., Tokyo, Japan) and after capping 6 ml of PFP was injected. A shaking machine (Ultra Mate 2, Victoria, Australia) was used to obatin bubbles. The temperature in the samples was measured after agitation using a needle-type thermometer (Custom Co., Tokyo, Japan). PFP content measurment was performed as reported in Section I 1. The particle size and zeta potential of the liposomes and bubbles were determined using a Zetasizer Nano ZS instrument (Malvern Instruments Ltd., Worcestershire, UK).

I.2.2.3. DOX binding efficiency

To determine the binding efficiency of DOX in DLBs, a sample consisting of 0.5 ml DLB's dispersion (1.65 mg lipid and 0.33 mg DOX) was centrifuged at 16,000 g for 2 min. Then the sample was divided into three fractions: a foaming cake at the top which contained DLBs; a pellet at the bottom, which contained liposomes; and in-between a solution containing free DOX. The fractions were collected, and then the concentration in each fraction was determined by measuring fluorescence of DOX with an excitation wavelength of 480 nm and emission wavelength of 590 nm (FluoroMax4, Horiba, Ltd., Kyoto, Japan).

I.2.2.4. *In vitro* echogenicity

The DLBs were injected into a beaker filled with 500 ml of degassed distilled water at 37°C under magnetic stirring. Ultrasound contrast enhancement was observed using an ultrasonography system (Vevo 2100, Visual Sonics, Inc. Toronto, Canada). For examination of DLB's destruction by higher energy TUS irradiation, an external TUS probe at an intensity of 2 W/cm² was used. The process of TUS burst was repeated until most of the DLBs had disappeared.

I.2.3. Results

I.2.3.1. Size and morphology of DLBs

The size of the DLBs was adjusted by changing the agitation time of the shaking machine. Agitation for 60 s was sufficient to produce bubbles with an average diameter of 1 μm (Table 1). During this procedure, the temperature did not exceed 26.7°C.

Table 1. Mean particle size and zeta potential of liposomes and bubbles. n = 3; mean ± SD

	Mean particle size (nm)	Zeta potential (mV)
Unloaded liposome	250 ± 1	-0.076 ± 0.02
DOX-loaded liposome	270 ± 6	0.038 ± 0.02
Unloaded bubbles (ULBs)	1051 ± 4	-0.066 ± 0.04
DOX-loaded bubbles (DLBs)	1022 ± 5	0.31 ± 0.01

I.2.3.2. Gas leakage

PFP gas retention was enhanced by the increasing of DOX content from 10 to 82%. The time course of gas leakage showed that at a DOX concentration of 10%, PFP gas leaked faster than bubbles without DOX. However, at levels of 42% and 82% (equivalent to 1:1 mole of DOX: DSPG) DOX enhanced PFP gas retention was evident for at least 30 min at room temperature relative to both ULBs (0 DOX) and the control (saline with PFP) (Fig. 5).

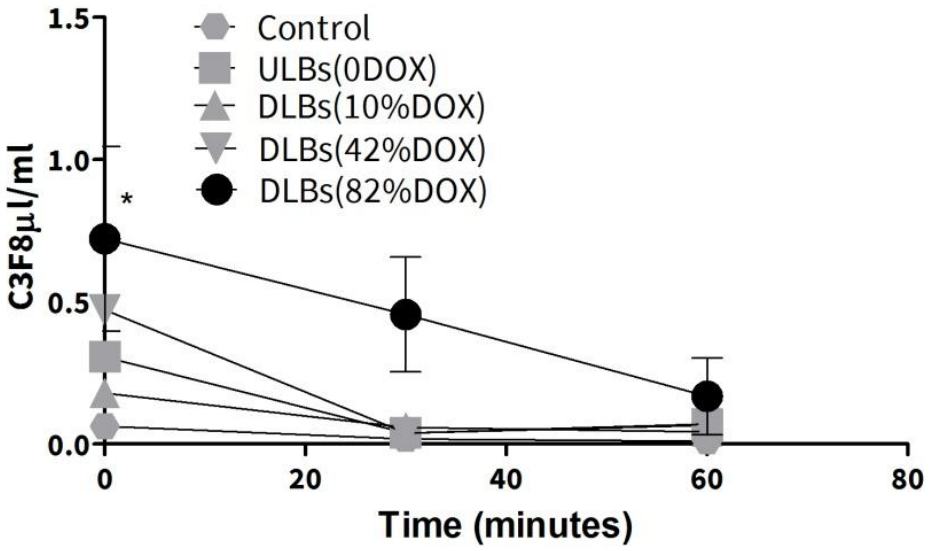

Fig. 5. Time course study of gas leakage from DLBs with different DOX concentrations presented as percentages equivalent to anionic phospholipids. Mean ± SEM. * $P < 0.05$ versus the corresponding control group (saline with PFP gas).

I.2.3.3. DOX loading efficiency

The loaded amount of DOX in DLBs was adjusted to 497.9 ± 17.4 µg/ml (n = 3), and 92.5% of the total DOX was loaded into the DLBs after total separation from free DOX and pellets (Fig. 6A). The fluorescence microscope images indicated successful DOX loading. Images showed spherical bubble in which the DOX signal was observed in the shells (Fig. 6B).

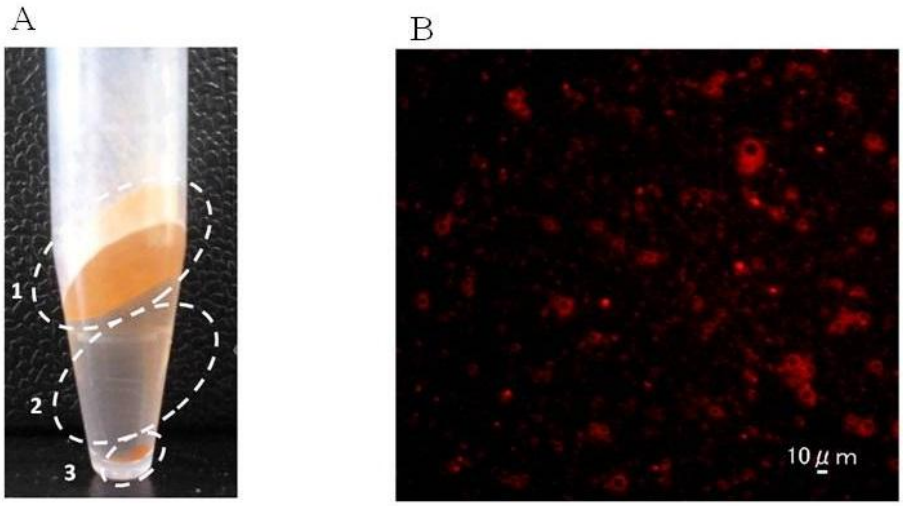

Fig. 6. (A). DLB's separation through buoyancy effects after centrifugation: (1) DLBs, (2) free DOX, and (3) pellets of phospholipids aggregate with doxorubicin. (B). Fluorescence images based doxorubicin detection (scale bar of 10 µm).

I.2.3.4. *In vitro* DLB's echogenicity and destructibility

The echogenicity of DLBs was assessed *in vitro* after injection of the freshly prepared DLBs at 37°C. The brightness mode of ultrasonography showed a high signal from the DLBs even after 10 min (Fig. 7A). The acoustic destructibility study for the DLBs demonstrated that TUS irradiation from 40 to 60 s caused a significant decrease in the ultrasonography video intensity as most of the bubbles had been destroyed (Fig. 7B).

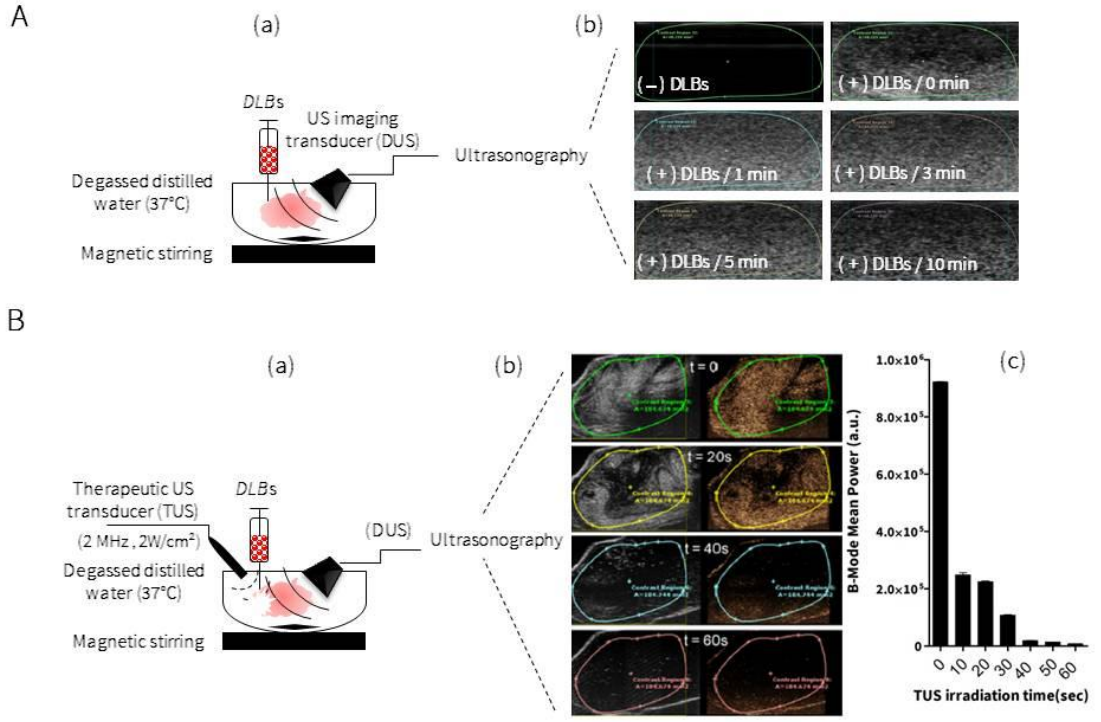

Fig. 7. (A). DLB's echogenicity *in vitro*: (a). US imaging experimental setup. (b). Images of DLBs in brightness mode. (B). *In vitro* DLB's acoustic destructibility. After the injection of DLBs, US echo imaging was performed and then the TUS destruction beam was applied from the external probe at an intensity of 2 W/cm^2: (a). US imaging experimental set up. (b). Images of DLB's brightness and contrast mode after the application of TUS irradiation. (c). Graph presenting DLBs contrast signal regression after 6 volumes of TUS irradiation (10 s each).

I.2.4. Discussion

Many studies have reported on the different methods by which DOX was successfully prepared and tested for tumour therapy in combination with TUS irradiation [21, 25]. Although most of the previous approaches achieved high therapeutic efficacy *in vitro* and *in vivo* [22, 23, 26], there is a little evidence regarding their potential role in US imaging and whether or not the co-encapsulation of PFP and DOX is effective enough for US contrast enhancement in addition to enhancement of

the therapeutic effect of DOX.

In this study, I examined the potential of the theranostics characteristics of DLBs. The size of DLBs was controlled by agitation and initially, 60 s of agitation was enough for producing bubbles with a good size distribution. This result indicates that the majority of DOX-phospholipids had formed DLBs with high DOX loading efficiency (92.5%).

During this procedure, the temperature did not exceed 26.7°C, suggesting that it is a mild process. This would be beneficial if thermo sensitive compounds are intended to be included in the formulations. The fluorescence images of DLBs revealed spherical shapes in which DOX was bound to the DSPG in the shell through electrostatic interactions between the positively charged DOX and the negatively charged bubbles (Fig. 6).

Since DOX loading and PFP gas retention are critical factors for the successful theranostic application, I attempted to investigate a possible relationship between PFP gas retention and the amount of DOX intercalated with DSPG in the bubbles. Gas chromatography was used to quantify the amount of PFP gas in the DLBs at different DOX to DSPG ratios. As shown in Fig. 5, a higher DOX loading enhanced PFP gas retention in the DLBs. These observations suggested that not only DSPG incorporation in bubbles but also the interaction between DSPG and doxorubicin is an important factor for stable PFP encapsulation.

TUS burst for a period of 60 s at an intensity of only 2 W/cm^2 was sufficient to induce a significant decrease in the contrast signal of DLBs; the presumption was that destruction of the DLBs most likely occurred as a result of bubble cavitation (Fig. 7B). It can be concluded that TUS burst caused the bubble destruction through the

comparison between Fig. 7A and Fig. 7B. As shown in Fig. 7A, the same DLBs monitored with lower energy DUS without burst and bubbles remain after 10 min whereas the 2 W/cm^2 burst destroyed virtually all bubbles in 40 s.

In conclusion, DLBs clearly showed therapeutic and diagnostic chracteristics due to high DOX loading into bubbles which also enhanced PFP gas retention. Additionally, DLBs could effectively interact with both TUS and DUS. Therefore, DLBs has the fundamental characteristics to be further utilised in cancer theranostics.

Section I. 3

The development of freeze-dried doxorubicin loaded bubbles

I.3.1. Introduction

In section I 2, I have demostrated that high amounts of DOX could successfully be loaded into bubbles. Also, DOX incorporation has improved PFP gas retention in bubbles as well. However, these bubbles should be freshly used during specific time window that usually varies between several hours and few days depending e.g. on the storage temperature. For the clinical relevance, the long term preservation and shelf-life of bubbles as dosage form is of importance. Therefore, I aimed from this study to improve the stability and shelf-life of DLBs by freeze-drying of the bubbles.

Freeze-drying, also known as lyophilization, is a common technique for preserving pharmaceutical dosage forms. In this process, ingredients are dehydrated by freezing step followed by heating at low pressure. Consequently, the frozen liquid in the bulk transfer to gas and dried porous state materials remain [28, 29]. By using this technology it was reported that bubbles could effectively be preserved for longer self-life by the addition of some lyoprotectants [30]. In fact, most of the commercially UCAs are available as dry state bubbles that have been preserved by freeze drying and can be easily re-constituted by addition of water [31, 32, 33].

In this section, the possibility of the long term preservation of DLBs by freeze-drying technology was investigated. The theranostic characteristics of DLBs after freeze-drying was tested and compared to that in fresh DLBs.

I.3.2. Materials and methods

I.3.2.1. Phospholipids

DSPG, DPPC and PEG_{2000}-DSPE were purchased from Avanti Polar Lipid Inc. (Alabaster, AL, USA) and NOF Co. (Tokyo, Japan). Sucrose was purchased from Wako Pure Chemical Industries, Osaka, Japan.

I.3.2.2. DLBs preparation

DPPC, DSPG and PEG_{2000}-DSPE are employed at 70:25: 5 molar ratio. Lipids were weighed and dissolved in MeOH: chloroform mixture. The solvent was removed by rotary evaporator and the sample was dried completely in vacuum over night. The dry lipid was hydrated with distilled water to a lipid concentration of 4 mM and heated at 65°C for 30 min followed by sonication for 10 min. The dispersion was diluted to 1mM and 20 ml was put in a 50 ml falcon tube. A mechanical rotor-stator type homogenizer (Ika T25 digital Ultra Turrax with S25 KV-18G gas tight dispersing element, Ika Werke GmbH, Staufen Germany) was placed with the dispersing element in the lipid dispersion and the tube was sealed with paraffin film. Using a tube the air was replaced by PFP. The sample was homogenised for 5 min at 15k rpm while PFP was continually pumped in (12 ml/min) to ensure the PFP atmosphere.

I.3.2.3. Freeze-drying

One millileter of bubble dispersion was mixed with 1 ml of 18% (w/v) sucrose solution in 5 ml vials. The air in the vials was replaced with PFP and the vials were sealed. In some samples the gas pressure was lowered to 0.5 atm by withdrawing some gas before freezing in -30°C freezer for 2hr. After completely frozen, the samples were transferred to a freeze-dryer with a temperature controlled drying chamber (Eyela FDU-1100 and Eyela DRC-1100, Tokyo Rikakikai co. Ltd., Tokyo, Japan) operating with a temperature program of -35°C, 1hr; -15°C, 8hr; +20°C, 8hr. After freeze-drying, the

vials were filled with PFP, sealed and kept in room temperature until use.

I.3.2.4. DOX binding efficiency after freeze-drying

To determine the binding efficiency of DOX in lyophilized DLBs (LDLBs), a sample consisting of 0.5-ml dispersion (200 ml LDLBs in 300 ml distilled water or lysis buffer) was prepared. Sample was added to 100 K filter centrifugation tubes (Merck Millipore. Ltd., Cork, Ireland) and then centrifuged at 14000 g for 7 min. After centrifugation, DOX level at the bottom of tubes was optically observed.

I.3.2.5. *In vitro* echogenicity

Similar to the *in vitro* echogenicity study in Section I 2, LDLBs were injected into a beaker filled with 500 ml of degassed distilled water at 37°C under magnetic stirring. Ultrasound contrast enhancement was observed using an ultrasonography system (Vevo 2100, Visual Sonics, Inc. Toronto, Canada).

1.3.3. Results

1.3.3.1. DLBs characteristics after freeze-drying

After freeze-drying, the lyophilized DLBs were clearly seen as a dried porous cake in the vial (Fig. 8A). The average size of freshly prepared DLBs was 488.7 nm. After freeze-drying and re-constitution with distilled water bubbles had an average size of 456.5 nm (Fig. 8B). Furthermore, DOX loading into bubbles after freeze-drying was confirmed. In this experiment, only LDLBs sample that mixed with lysis buffer resulted in DOX elution after centrifugation. On the other hand, there was no significant appearance of DOX in elutes after centrifugation in that mixed with distilled water only (Fig. 8C).

1.3.3.2. *In vitro* echogenicity

Both freshly prepared DLBs and LDLBs had high and distinguishable contrast signal compared to DOX unloaded bubbles (ULBs). Also it was noticed that decreasing the pressure inside vials from 1 to 0.5 atm can enhance the LDLBs contrast for longer time (Fig. 9).

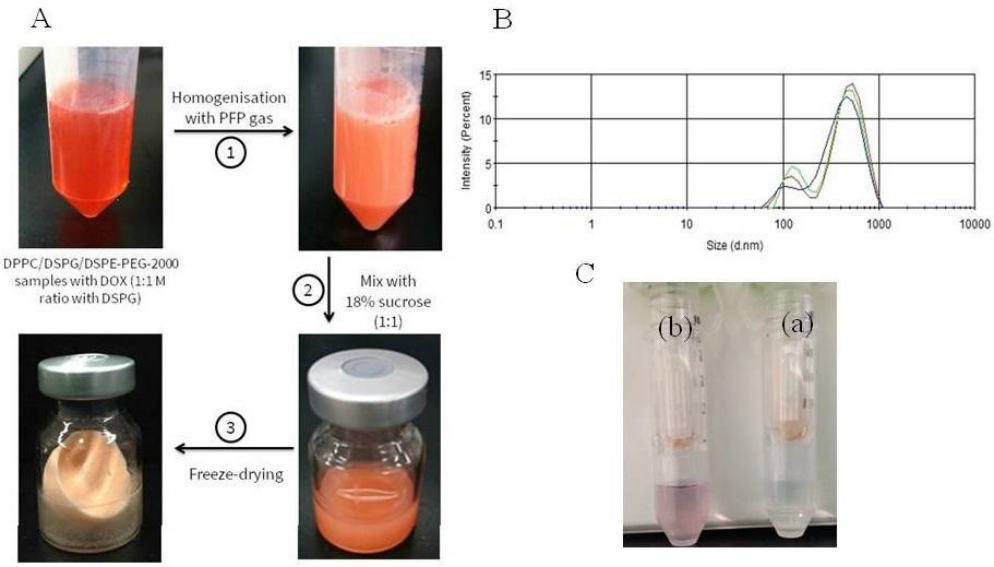

Fig 8. The characterization of lyophilized DOX loaded bubbles. (A). Stepwise protocol for preparing LDLBs. (B). Size distribution histogram of LDLBs after re-constitution in distilled water. (C). Diluted LDLBs after centrifugation; (a) LDLBs in distilled water (b) LDLBs in lysis buffer.

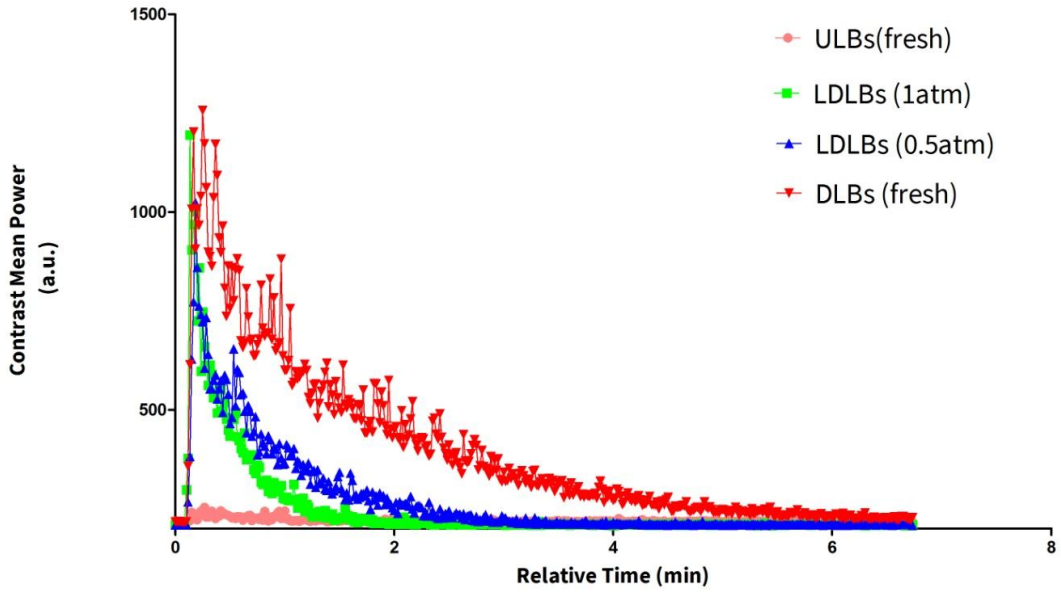

Fig 9. *In vitro* echogenicity of DLBs before and after freeze-drying.

I.3.4. Discussion

For clinical use, the preservation of dosage forms for longer shelf-life is critical. In the present study, I demonstrated, to the best of my knowledge, the first attempt in preparing lyophilized DOX loaded bubbles (LDLBs). Bubbles were freeze-dried in the presence of sucrose as cryoprotectant. The re-constitution in distilled water following with a gentle shake for few seconds was enough for producing bubbles again. The size of LDLBs did not change after freeze-drying. Moreover, DOX was still loaded into bubbles after freeze-drying. It was reported that the addition of sugars is conditional for preserving the self assembly in particles structures. Sugars have the ability to form an amorphous glassy matrix that protect the vesicle structure from the stress and damage during freeze-drying or even after the re-constitution with water [33]. And in case of bubbles, it was also reported that lyophilized bubbles with glucose or sucrose could maintain the structure and echogenic properties after freeze-drying [29]. The current results indicated that the sucrose could preserve the phospholipids-DOX structure after freeze-drying.

Similar to the findings in Section I 2, DOX loading into bubbles enhanced their echogenicity compared to ULBs (no DOX). Indicated again that DOX loading into phsopholipid shell of bubbles might have delayed the lateral gas diffusion hence bubbles could be more stable. Moreover, the echogenicity of LDLBs was further improved by adjusting the gas pressure inside the vials. At 0.5 atm LDLBs tended to have better echogenicity profile. The reason for this is unclear though and needs to be investigated in further studies. In this study, most of the LDLBs samples were tested in time range between 1-2 months after freeze-drying. Therefore, information of long term stability of LDLBs (~1 year) might be needed and considered in future.

In conclusion, LDLBs were successfully preserved by freeze-drying technique suggesting that this method might be used for enhancing the shelf-life of phospholipid-based theranostic UCAs. Additionally, the previous finding could open the door for further investigations related to similar theranostic UCAs systems loaded with bioactive molecules such nucleic acids or even different macromolecules.

Section I. 4

Phospholipid-based phase shift acoustic nano-droplets

I.4.1. Introduction

Passive tumour targeting by nanocarriers is common. In this approach, tumour accumulation is achieved through the involvement of the enhanced permeability and retention (EPR) mechanism. To achieve this, particles should be sustained in the circulation for a long time. Particles could then passively cross the defaced inter-endothelial gaps in tumour microvasculatures [34]. Due to the lack of lymphatic drainage in the tumour, particles can be further retained and trapped inside the tumour. In section I 1 and 2, I showed that bubbles type of UCAs could be stably formed and characterised for theranostic uses. However, the size of these bubbles was in a range between 400-1000 nm in diameter. For achieving EPR effects, however, particles should have small size such as 100-200 nm in addition to long stability *in vivo* [35]. Several reports have shown that smaller bubbles could possibly be formed and utilised in cancer theranostics [5, 36]. These bubbles usually have a short stability that limits the EPR effects. Bubble instability can in part be explained according to Young-Laplace equation:

$$\Delta P = (P)inside - (P)outside = \frac{2\sigma}{r} \qquad (1)$$

Where P is the pressure, σ is the surface tension and r is the radius. By decreasing the bubbles size the pressure inside the bubbles will increase and that means the gas inside the bubble will leak more quickly. As a result bubble will soon dissolve and dissipate [15, 16, 37]. Therefore, producing small bubbles that have diameters of about 100-200 nm and stable for a long time is obviously difficult. An alternative solution has been done

by introducing the concept of bubbles precursors. It's also known as phase shift acoustic nano-droplets (PSANDs). The idea includes the use of PFCs with a high boiling point such as perfluoropentane (PFPn~29 ºC) and perfluorohexane (PFH~56 ºC). These PFCs are stable at the room temperature [38, 39]. The emulsification of liquid PFCs with specific surfactant such as phospholipids lead to the formation of nano-droplets. Under the thermal or acoustic effects of therapeutic ultrasound (TUS), droplets can then be activated in situ by enforcing the phase shift transition from liquid to gas. And bubbles can be generated [40, 41]. Taking these in consideration, I aim from this study for developing phospholipid-based PSANDs with small size and high stability adequate for the purpose of cancer theranostics.

In this section, PSANDs were made with a similar phospholipid composition as in section I 1, and with the use of PFPn or PFH. Size, stability, and sensitivity towards TUS were investigated for better theranostic assessment.

I.4.2. Materials and methods

I.4.2.1. Phospholipids

DSPC was purchased from Avanti Polar Lipid Inc. (Alabaster, AL, USA) and PEG-$_{2000}$-DSPE was purchased from NOF Co. (Tokyo, Japan).

I.4.2.2. PSANDs preparation

DSPC and PEG-$_{2000}$-DSPE in a 94:6 molar ratio were dissolved in chloroform, followed by evaporation of the chloroform in a rotary evaporator; this was further dried under vacuum at room temperature overnight. The lipid film (8 mg/ml) was hydrated with PBS solution at 65°C for 60 min under mild agitation followed by sonication with bath sonication for 3 min and then tip sonication type for 2 min. For preparing droplets, 1

ml of liposomes was added to a 2 ml sterilised vial followed by adding 60 µl of PFH or PFPn (sigma-Aldrich). The vial was capped and exposed to bath type sonication for 3-5 min on ice. The sample was kept at 4 °C for further use.

I.4.2.3. Characteristics of PSANDs

The particle size and zeta potential of the liposomes and PSANDs were determined using a Zetasizer Nano ZS instrument (Malvern Instruments Ltd., Worcestershire, UK). The number of PSANDs was estimated using the formula:

$$N = \frac{V \times Fr \times 10^9}{\frac{4\pi r^3}{3}} \qquad (2)$$

Where N is the number of PSANDs, V is the volume of PFCs in (µl), Fr is the fraction of selected size distribution, and r is the radius in µm. In the calculation, the loss of PFCs during preparation and the shell thickness was considered negligible.

I.4.2.4. *In vitro* echogenicity

Rubber tube was fixed in a pre-heated bath water at 37°C. One and half millilitres of distilled water was added into the tube and then left for 10 min for temperature equilibrium. A diagnostic ultrasound transducer (DUS) was fixed at the edge of the rubber tube and then three images were taken. After that, 10 µl of PSANDs was added and mixed well with a pipette. An external therapeutic US (TUS) transducer was immersed in the rubber tube so that it did not interfere with the ultrasonography probe. TUS irradiation has been applied in different frequencies, intensities and exposure time separately followed by taking another three images. US signal enhancement values were analysed as the contrast brightness values after TUS irradiation minus contrast/ brightness values before TUS irradiation.

I.4.2.5. *In vitro* PSANDs stability at physiological temperature

For evaluating the stability under the physiological conditions, PSANDs were challenged against physiological temperature. Briefly, 100 µl of PSANDs was mixed with 500 µl PBS. Samples were placed in water bath at 37° C and 10µl sample was collected at different time points for PFH and PFPn quantification. Samples were analysed by using gas chromatography (GC) as reported in Section I1.

I.4.3. Results

I.4.3.1. Characteristics of PSANDs

PSANDs could be prepared without any phase separation or creaming (Fig. 10A). PSANDs had an average size of around 200 nm and neutral zeta potential (Table 2). However, droplets that were made with PFH tended to have a more narrow size distribution compared to that made with PFPn (Fig. 10B). The number of droplets (N) according to formula (1) was estimated to be 1.43×10^{13} per ml of the prepared sample considering a radius of (r = ~0.1µm) and the volume of PFH or PFPn in 1 ml of the sample (V= 60 µl).

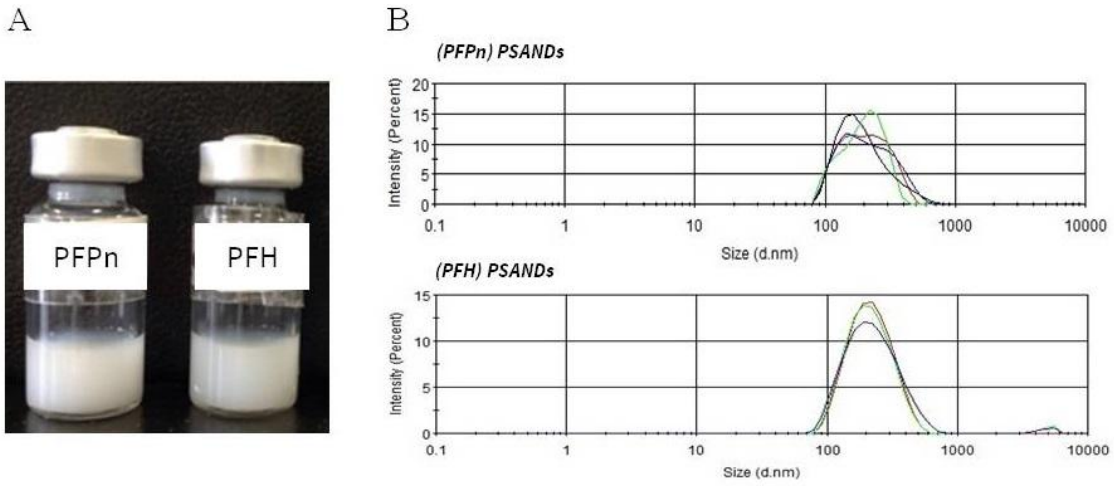

Fig. 10. (A). PSANDs after emulsification. (B). Size distribution histograms of PFPn PSANDS and PFH PSANDs; (n= 3-4 measurements)

Table 2. Mean particle size and zeta potential of liposomes and droplets. n = 3; mean ± SD

	Liquid perfluorocarbon	Particle size (nm)	Zeta potential (mV)
Liposome (DSPC;PEG-$_{2000}$-DSPE)	—	101 ± 1.0	0.069 ± 0.04
PSANDs(PFPn)	C_5F_{12}	194 ± 6.5	0.023 ± 0.01
PSANDs(PFH)	C_6F_{14}	205± 1.8	0.023 ± 0.08

I.4.3.2. *In vitro* echogenicity

Ultrasonography was used to investigate the phase transition of droplets to bubbles *in vitro*. The extent of phase shift depended more on the TUS frequency than the intensity. Maximum contrast enhancement was achieved with TUS intensity of about 2 W/ cm^2 and for PFPn, and 5 W/ cm^2 for PFH PSANDs (Fig. 11A, B, and D). On the other hand, PSANDs that were irradiated with 3 MHz TUS in did not induce any contrast signal. Increasing US intensity also had no impact on the phase transition of droplets (Fig. 11C).

I.4.3.3. *In vitro* PSANDs stability at physiological temperature

Both PFPn/ PFH leakage from PSANDs was tested *in vitro* at 37 ºC. GC quantification showed that both PFPn and PFH were retained in droplets at least for 1 hr (Fig. 12).

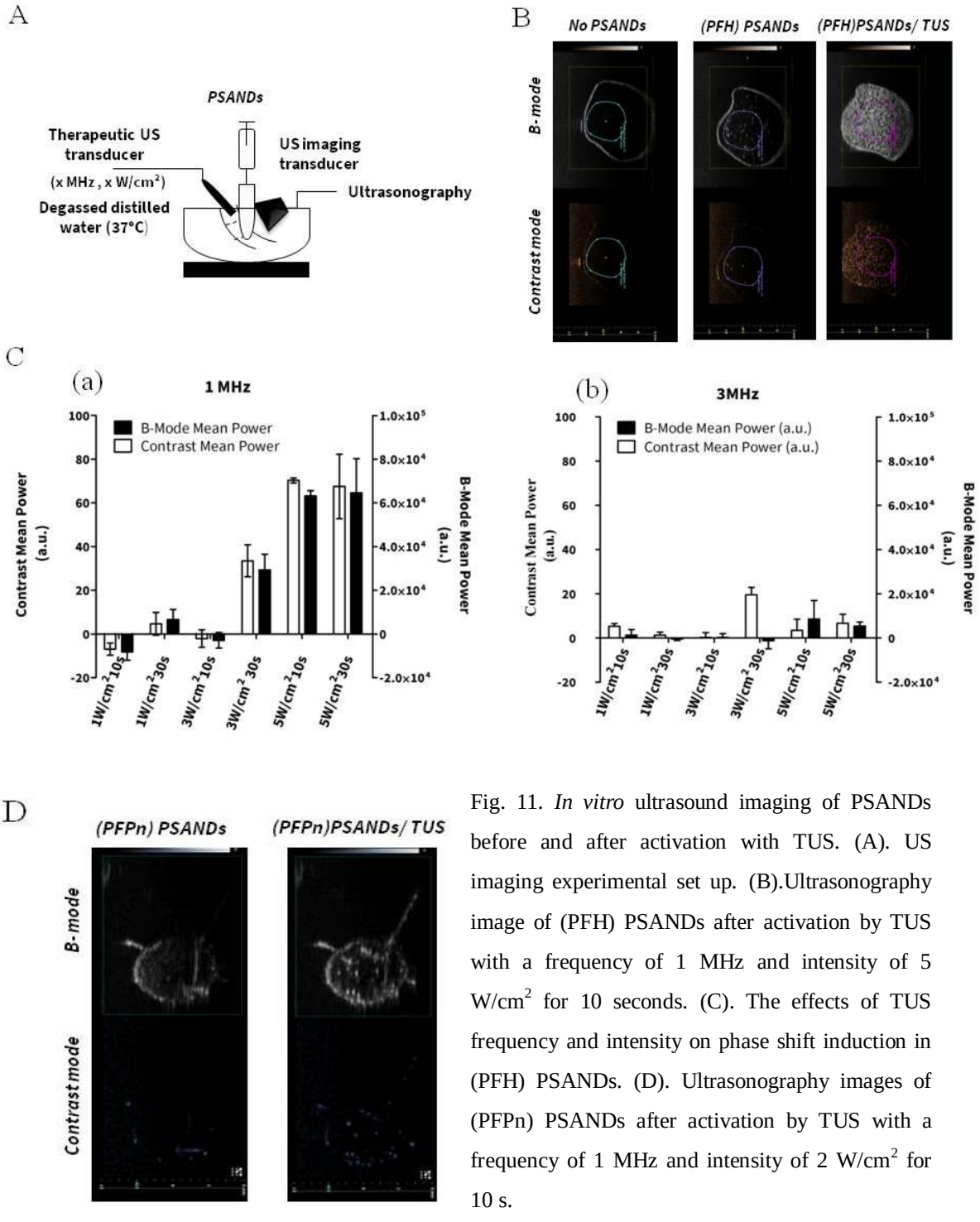

Fig. 11. *In vitro* ultrasound imaging of PSANDs before and after activation with TUS. (A). US imaging experimental set up. (B).Ultrasonography image of (PFH) PSANDs after activation by TUS with a frequency of 1 MHz and intensity of 5 W/cm^2 for 10 seconds. (C). The effects of TUS frequency and intensity on phase shift induction in (PFH) PSANDs. (D). Ultrasonography images of (PFPn) PSANDs after activation by TUS with a frequency of 1 MHz and intensity of 2 W/cm^2 for 10 s.

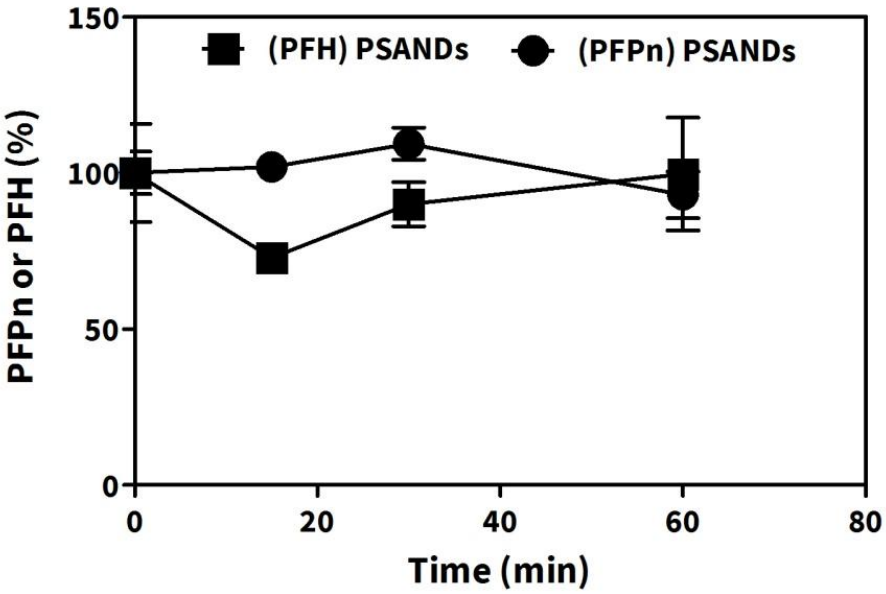

Fig. 12. *In vitro* PSAND's stability at 37 ^{O}C. Both PFPn and PFH nanodroplets were incubated in PBS at 37 C, and samples at specific time points were collected for gas chromatography (GC-MS) analysis of PFPn and PFH. n = 3; mean ± SEM

I.4.4. Discussion

In this section, I showed that PSANDs can be successfully prepared in a nanometer-scale range. Based on the phospholipid composition that I have utilised in section I 1, I could produce bubbles precursors. This was achieved by utilising the liquid perfluorocarbons such as PFPn and PFH. Droplets were formed by using bath type sonication on ice. The produced droplets were homogenous in size with a narrow distribution. Rapport et al and others reported that droplets can be formed in average size of several hundreds of nanometers. In these reports block copolymers and fluorinated surfactant was used to stabilise droplets [42, 43, 44]. My results indicated that the use of zwitterionic phospholipid (DSPC) with a portion of DSPE-PEG2000 was also effective for stabilising droplets. Moreover, droplets tended to have smaller size and more homogenous distribution.

To evaluate PSAND's stability under the physiological condition, the leakage of PFPn and PFH from droplets was tested *in vitro* at 37 ^{O}C. PFPn and PFH were completely retained in droplets at least for 1 hr. Although PFPn is supposed to be evaporated at 37 ^{O}C since boiling point is ~29^{O} C, the results showed complete retention of PFPn in droplets. This can be explained also in accordance with Laplace pressure equation. PASNDs were already stabilised with phospholipids that reduce the surface tension between liquid PFPn and the surrounded bulk liquid. On the other hand, Laplace pressure is reversibly proportional to the droplets size. And as droplets get smaller the pressure inside becomes greater. This means that in both PFPn and PFH, boiling point will be then increased above original values [45]. In general, these results indicated that PSANDs can still remain stable at the physiological temperature. In another word, PSANDs might remain inactivated as bubbles precursors in the circulation.

The acoustic droplets vaporisation (ADV) *in vitro* was achieved with TUS in a frequency of 1 MHz selectively. The ADV threshold was also depending on the type of PFCs that PSANDs made of. Basically, (PFH)PSANDs required higher TUS intensity (5 W/cm2). That can be related to the variances in the final boiling points between PFPn and PFH inside the droplets. These results implied that PSANDs can be activated exclusively by TUS possibly without interface with the diagnostic ultrasound (DUS) that usually used in frequencies more than 2.5 MHz [46].

In conclusion, this study showed that PSANDs can be prepared with small size and high stability at the physiological temperature. Additionally, PSANDs showed selective sensitivity toward TUS. Therefore, these UCAs might valuably contribute in cancer theranostics after systemic or local administration.

Chapter II

Application of phospholipids-based ultrasound contrast agents in gene delivery and cancer theranostics

Section II. 1

The effective use of mechanically formed bubbles in enhancing the gene delivery

II.1.1. Introduction

Enhancing the delivery of nucleic acids is a major task in the field of drug delivery research. The delivery of naked plasmid DNA (pDNA) is made difficult by the size, hydrophilicity and anionic charge of the pDNA molecule, all reducing its uptake through the cellular membrane. Also, as an additional difficulty, pDNA is unstable *in vivo*; owning to its rapid degradation. Many transfection methods have been introduced recently such as viral vectors and cationic liposomes [47, 48]. In spite of their high efficiency, sill these approaches have some unfavoured properties such as cytotoxicity and immunogenicity [49]. Ideally, the pDNA should be delivered to the cytosol of cells but most carriers are taken up by endocytosis and that limits the level of gene expression because of degradation in lysosomes [49]. Ultrasound contrast agents (UCAs) such as microbubbles (MBs) and nanobubbles (NBs) have been reported to be effective in enhancing the delivery of nucleic acids directly to the cytosol due to sonoporation. Sonoporation is the process that UCAs in combination TUS irradiation lead to temporary pores in the cellular membrane. This process facilitates the direct delivery of pDNA to the cytosol without endocytosis [50, 51, 52]. Moreover, UCAs have unique properties that can be used as advanced carriers in drug delivery. The biocompatible shell made of phospholipids, proteins, or polymers can be loaded with drug or nucleic acids. The gas core makes it easy to detect the carrier with contrast mode US imaging and also makes it possible to trigger cavitation needed for sonoporation leading to site-specific activation [53, 54]. The advantage of NBs over MBs is mainly the smaller sizes that favour them with better distribution in the blood

circulation. These small bubbles can then cross through tiny vasculature that has diameters less than 1 micrometre [36, 55]. Also, the smaller sizes of NBs can reduce the chances of the clinical complications such as vessel blockage and embolism risks [56]. Moreover, it has been reported that bubble stability can determine the *in vivo* gene transfection [57]. In Section I 1, I showed that mechanically formed bubbles (MFBs) can be stably prepared in sizes of a few hundred nanometires. Bubbles had homogenous and narrow size distribution. Based on that, I aimed in the current study to evaluate the potential use of MFBs in enhancing the gene delivery both *in vitro* and *in vivo*.

In this study, I investigated the potential of MFBs for more efficient sonoporation leading to plasmid DNA uptake both *in vitro* and *in vivo* and also the related efficacy to the stability of MFBs.

II.1.2. Material and methods

II.1.2.1. Cells and plasmid DNA

The C26 murine colon adenocarcinoma cell line was obtained from the American Type Culture Collection (ATCC, Manassas, VA, USA). Cells were cultured in Dulbecco's modified eagle medium Nissui Pharmaceutical Co., Ltd., (Tokyo, Japan) supplemented with 10% fetal bovine serum and 100 U/ml penicillin/streptomycin at 37ºC in 5% CO_2. The pCMV-Lu was constructed by subcloning the HindIII/Xba I firefly luciferase cDNA from pGL3 control vector (Promega, Madison, WI, USA). The pDNA was extracted using Endofree Plasmid Giga kit (QIAGEN GmbH, Hilden, Germany).

II.1.2.2. Animals

Female 6-week-old ICR mice were purchased from the Shizouka Agricultural Cooperation Association for Laboratory Animals (Shizouka, Japan). All experiments

were approved by the animal Experimentation Committee of the Graduate School of Pharmaceutical Sciences, Kyoto University.

II.1.2.3. *In vitro* gene transfection into Colon C26 cells

Colon C26 cells were suspended (1×10^4 cells/500 µl) in RPMI medium supplied with 10 % FBS in 48 well plate. MFBs (15 µg) and pDNA (3 µg) were mixed and added to cells. TUS was applied for 10 and 20 s (2 MHz; 2.5 W/cm²; 50% duty; 10 Hz). After treatment, cells were incubated for 15 hr. For luciferase assay, the medium was discarded and cells were treated with lysis buffer (200 µl/well) on ice. Cell lysate was collected for luciferase assay using PicaGene Luminescence kit (Toyo ink Co., Ltd., Tokyo, Japan) and luminometer (Lumat LB 9507, EG&G Berthold, Bad Wildbad, Germany). Protein was quantified by protein quantification kit (Dojindo Molecular Technologies, Inc., Tokyo, Japan). WST-1 assay was determined by using WST-1 cell proliferation reagent (Roche Diagnostic Corporation, IN, USA). The absorbance was measured at 450 nm with a reference wave length of 620 nm using EON micro plate reader (BioTeck, Winooski, VT, USA).

II.1.2.4. *In vivo* gene transfection into limb muscles

Mice were intravenously injected with 200 µl and 400 µl of pre-mixed MFBs/ pDNA that contain 100 or 200 µg of lipids and 50 µg of pDNA. Immediately after injection, the left limb was irradiated with TUS using Sonopore 4000 (Nepa Gene CO., Ltd., Chiba, Japan) for 60 s (frequency 1 MHz; intensity 1W/cm²; duty 50%; burst rate 10 Hz). Six hours after injection mice were sacrificed and tissues were collected. Tissues were homogenised in lysis buffer (0.05% triton X-100, 2 mM EDTA, 0.1 M Tris; pH 7.8). Homogenised samples were then centrifuged at 10000 g for 8 min at 4 °C. Supernatants were collected and applied for luciferase assay using PicaGene

Luminescence kit (Toyo ink Co., Ltd., Tokyo, Japan) and luminometer (Lumat LB 9507, EG&G Berthold, Bad Wildbad, Germany). Protein was quantified by protein quantification kite (Dojindo Molecular technologies, Inc., Tokyo, Japan).

II.1.2.5. Statistical analysis

All data was analyzed as the mean ± SEM. Unpaired, the two-tailed distribution Student's t-test was applied, while multi-comparison with control was analyzed using Dennett's test. Values of $P < 0.05$ were considered as being statistically significant.

II.1.3. Results

II.1.3.1. *In vitro* gene transfection and WST-1 assay

The level of *in vitro* gene expression was tested in C26 cells. The result showed that gene expression was significantly enhanced with both MFBs/pDNA/TUS10s ($P < 0.05$) and MFBs/pDNA/TUS20s ($P < 0.05$). In contrast, pDNA only, pDNA/MFBs, pDNA/TUS10s and pDNA/TUS20s did not induce any significant increase in the level of gene expression (Fig. 13 A). WST-1 assay indicated no significant reduction in cell viability with TUS, pDNA only, MFBs/pDNA, and MFBs/pDNA/US10s. However, a significant decrease of cells was noticed when cells were treated with MFBs/pDNA/US 20s ($P < 0.05$) (Fig. 13B).

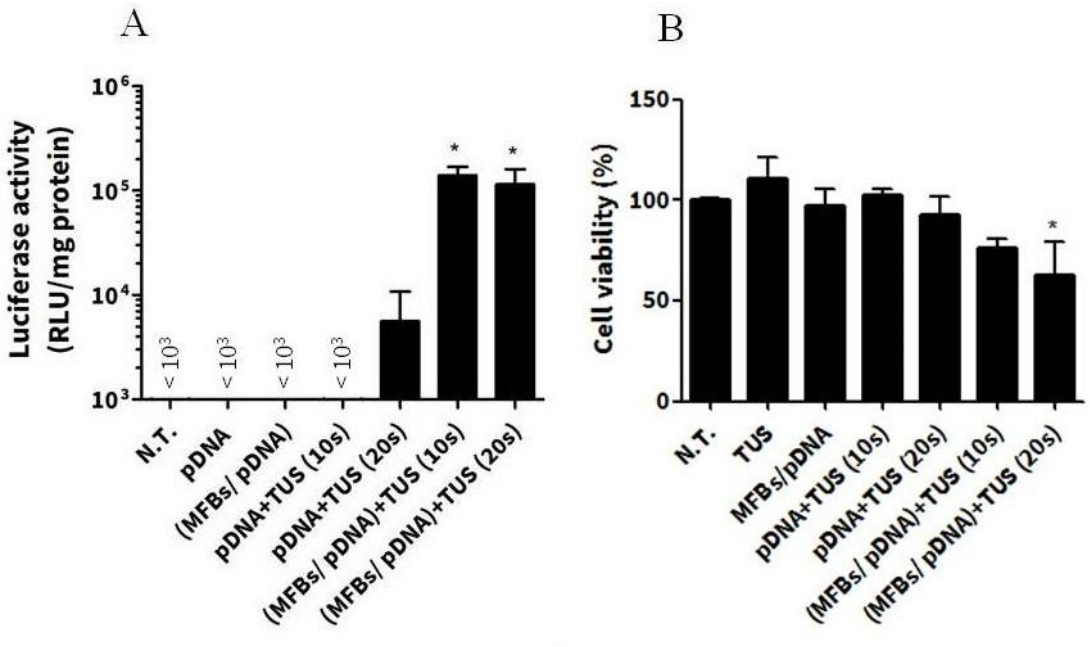

Fig.13. *In vitro* gene expression and cellular damage in C26 cells having various treatment with pDNA. (A) *In vitro* gene transfection. (B) WST-1 assay. Colon C26 cells were treated with MFBs with pDNA and TUS. Fifteen hours after transfection, cells were harvested and the level of luciferase was evaluated in addition to WST-1 assay. Each bar represents the mean ±SEM of 3-5 experiments. *$P < 0.05$ versus the corresponding group of no treatment (N.T.).

II.1.3.2. *In Vivo* gene expression in limb muscles

II.1.3.2.1. The effect of MFBs dose

For *in vivo* gene expression experiment, mice left limb muscles were selected as the TUS targeted site. MFBs were used in two doses: 100 µg lipid/200 µl and 200 µg lipid/400 µl. MFBs were capable of inducing significant increase of gene expression in both doses while mice treated with pDNA and TUS only gave no significant enhancement of the gene expression. For the other experiments, MFBs that contains 200 µg lipids was chosen as a dose, pre- mixed with pDNA, and intravenously injected (Fig. 14).

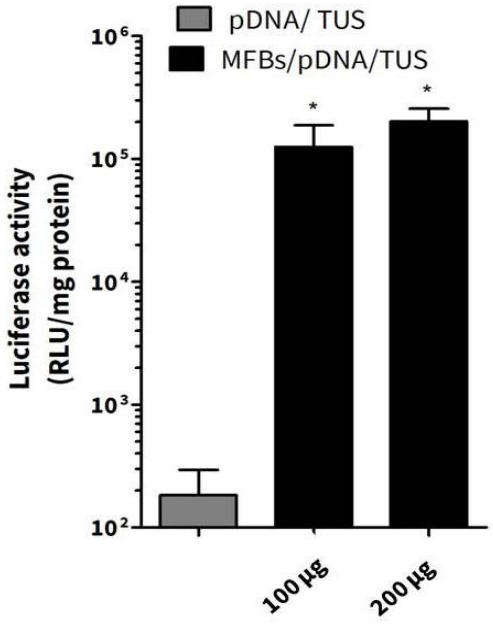

Fig. 14. *In vivo* gene transfection of pDNA in mice limb muscles having difffrent doses of MFBs. After *i.v.* injection of MFBs/pDNA, TUS was irradiated on the left limb area. Each bar represents the mean ± SEM of 3-6 experiments. * P <0.05 versus the corresponding group of pDNA/TUS.

II.1.3.2.2. Site-selective gene delivery by MFBs and TUS

The gene expression in different organs was investigated after the *i.v.* administration of MFBs/pDNA. The highest level of gene expression was found in the left limb muscles that have been irradiated with TUS (P <0.0001; left limb versus different Tissues). In contrast, other tissues that had not been irradiated with TUS expressed low levels of the luciferase activities (Fig. 15).

II.1.3.2.3. The effect of MFB's stability on gene transfection

MFBs that were kept at the room temperature and at specific time points were mixed with pDNA and administrated into mice followed by TUS irradiation on the left limb muscles. The group of animal (n = 3- 6) that were treated with MFBs/pDNA in combination with TUS had a significant higher level of gene expression compared with that having only pDNA in combination with TUS irradiation (n = 4). After 2 hr the level of expression was slightly decreased. However, the level of expression was still significantly higher in groups treated with 24 hr aged MFBs/pDNA and TUS (P <0.05)

compared with mice treated with pDNA and TUS only (Fig. 16). MFBs that were stored at 4 ℃ for 90 hr were also tested for their ability in inducing transfection when combined with pDNA and TUS. Although the gene expression was somewhat lower than the groups treated with freshly prepared MFBs or even with those kept for 24 hr at RT, still the level of gene expression was significantly higher (P<0.05) compared with mice treated with pDNA and TUS only (Fig. 16).

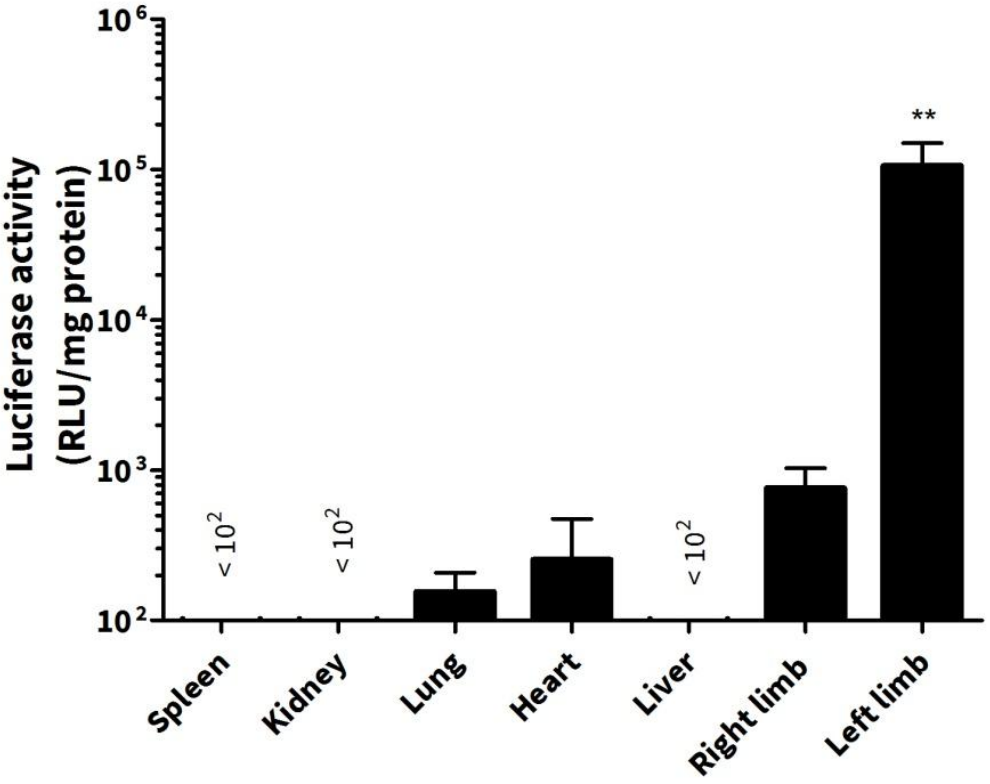

Fig. 15. *In vivo* tissue selective gene transfection in mice limb muscles in comparison with other organs. After *i.v.* injection of MFBs/pDNA, TUS was irradiated on the left limb muscle. Each bar represents the mean ± SEM of 3-6 experiments. ***P* <0.0001versus all tissues.

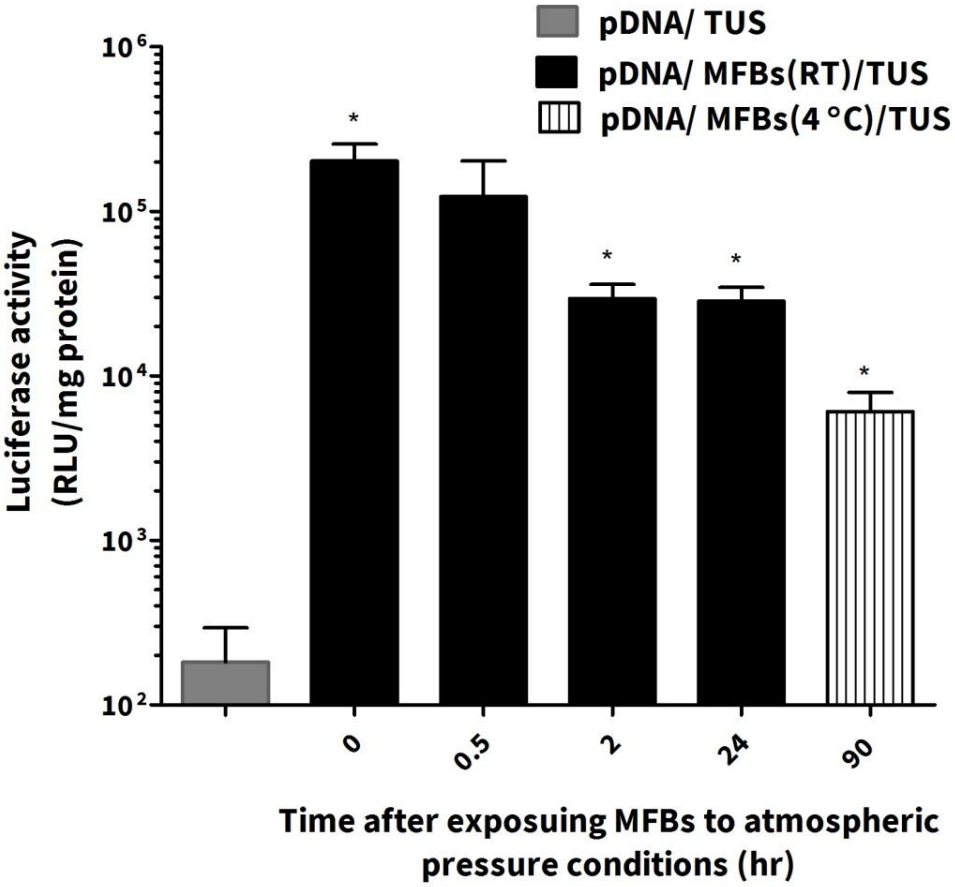

Fig. 16. The effect of MFBs stability on the *in vivo* gene transfection. Each bar represents the mean ± SEM of 3-5 experiments. * P <0.05 versus the group of pDNA/TUS.

II.1.4. Discussion

It has been clear that sonoporation with bubbles is an effective strategy for enhancing the gene delivery. The process includes the perturbation of cells' membrane leading to direct delivery of genes into the cytosol [58, 59]. To investigate such a concept, the *in vitro* gene transfection was evaluated in C26 cells. Ten seconds of TUS irradiation in combination with MFBs/pDNA was found to be sufficient for enhancing the gene expression without a significant increase in cytotoxicity. Further increase of TUS exposure time tended to induce some damage on cells. That can be due to the extensive bubble cavitation that might violently disrupt the cells' membranes and led to

cellular damage [60]. These results corresponded to a previous report with a similar experimental condition [61]. However, in this case, I achieved similar gene expression levels in C26 cells with a lower dose of bubbles (one fourth of bubbles dose). These differences might be related to the higher amount of perfluropropane encapsulation in MFBs that possibily affected bubble`s cavitation. Thus, these results indicate that MFBs can induce sufficient enhancement in gene transfection when combined with TUS irradiation.

In vivo conditions involve many critical factors such as shear stress and further gas exchange between bubbles and dissolved gases in blood that will add an extra burden on the bubbles [62, 63]. Consequently, sonoporation can be affected by bubble condition and thus uptake of pDNA as well [57]. Therefore, I tested both fresh and aged MFBs *in vivo* in mice. The gene expression was specifically enhanced in the left limb muscles of mice treated with MFBs/pDNA/TUS. In others organs, the gene expression level was not significantly changed. These results showed the effectiveness and usefulness of MFBs in inducing tissue-selective gene transfection. Moreover, aged MFBs that were stored at room temperature for different periods were tested in combination with TUS. The results showed that aged MFBs that kept at RT were effective in enhancing the gene expression even after 24 hr when combined with TUS. Furthermore, MFBs that were stored at 4 ºC for 90 hr were also able in inducing some cavitation effects. These results confirmed that aged MFBs can still have the potential in inducing sonoporation effects *in vivo* depending on the preservation conditions.

In conclusion, MFBs showed a strong ability in enhancing the gene transfection after systemic administration in combination with TUS suggesting the important role of MFBs in enhancing gene delivery.

Section II. 2

Evaluation of the theranostic potential of doxorubicin loaded bubbles in tumour bearing mice

II.2.1. Introduction

Cancer theranostics is a portmanteau of cancer therapy and cancer diagnostics. It is usually done through the co-delivery of the anti-cancer agents together with the contrast imaging agents. The aim of such strategy is the active monitoring of cancer progress during therapy [64, 65]. A more advanced approach is to put the therapeutic function and the diagnostic function in the same carrier. In such a case trade-offs between the diagnostics and therapeutic functions may have to be done to get balanced theranostic characteristics. The combination between UCAs and TUS/DUS can provide a novel, non-invasive platform for cancer theranostics [50, 66]. The main benefits of using TUS activated bubbles for various therapeutic applications are that the effect can be localised to primarily the tissues that are exposed to TUS and that the bubbles are also possible to be detected with DUS imaging. The imaging aspect can be used for *e.g.* examination of tumour neovasculature but also the treatment itself can directly be assessed by *e.g.* monitoring bubble location and bubble destruction in real time at the target site [67, 68]. This concept has already been shown to have potential in many reports in mice with tumour models and results have confirmed that the concentration of anticancer drugs in the tumour can be increased when using such strategy [20].

In section I 2, the preparation of bubble type UCAs that were successfully loaded with high amount of DOX and PFP gas was described. The balance between the contrast gas and DOX loading was successfully achieved. Also, DLBs had high *in vitro* echogenicity in addition to the ability in inducing cavitation effects when combined

with TUS. Therefore, it is expected that DLBs could be an effective theranostic agent in cancer therapy.

In this study, both therapeutic and diagnostic tests were conducted *in vitro* with tumour cells and *in vivo* in tumour bearing mice. That included: DOX accumulation in tumour, tumour volume reduction, animal body weight change, and ultrasonography imaging of DLBs in tumours.

II.2.2. Materials and methods

II.2.2.1. DLBs preparation

Bubbles were prepared as described in Section I 2.

II.2.2.2. Cells

The B16BL6 murine melanoma cell line was obtained from the American Type Culture Collection (ATCC, Manassas, VA, USA). Cells were cultured in Dulbecco's modified eagle medium Nissui Pharmaceutical Co., Ltd., (Tokyo, Japan) supplemented with 10% fetal bovine serum and 100 U/ml penicillin/streptomycin at 37ºC in 5% CO_2.

II.2.2.3. Animals and tumour models

Female 6-week-old C57BL6 mice were purchased from the Shizuoka Agricultural Cooperation Association for Laboratory Animals (Shizuoka, Japan) and female 6-week-old HRI nude mice were obtained from Sankyo Laboratory Service Corporation, Inc. (Tokyo, Japan). For preparing tumour bearing mice, 1×10^6 cells in phosphate buffered saline (PBS) were injected subcutaneously into the left flanks of mice with a 26-gauge needle. Experiments were initiated when tumours reached 5–10 mm in diameter after 9–14 days. All experiments were approved by the animal Experimentation

Committee of the Graduate School of Pharmaceutical Sciences, Kyoto University and by Teikyo University School of Medicine Animal Ethics Committee number 14-027.

II.2.2.4. *In vitro* cellular uptake and anti-proliferative assay

Cellular uptake *in vitro* was evaluated using a confocal microscopy (Nikon, Tokyo, Japan). B16BL6 cells were grown on cover glass slides in 24-well plates (3×10^5 cells/well). DLBs were added to the medium, containing DOX at concentration of 5 µg/ml. Then a 6-mm TUS probe was immersed into the well and TUS irradiation was performed for 60 s (2 MHz; 2W/cm²; 50% Duty; 10 Hz). TUS acoustic parameters were selected based on the previous DLBs destructibility experiment described in Section I 2. Fifteen minutes after the treatment with DLBs and TUS, cells were washed with PBS three times and fixed with 4% paraformaldehyde in PBS; DOX localization in cells was then obtained. The 480 nm filter of the microscope was used to excite DOX and then DOX was detected by the 590 nm detector. The images were processed using ImageJ software.

As for anti-proliferative assay, B16BL6 cells were seeded in 6-well plates (3×10^5 cells/well) for 24 hr; DLBs/ULBs (0 DOX) were added at different concentrations. TUS was applied for 60 s (2 MHz; 2W/cm²; 50% duty; 10 Hz). After treatment, cells were incubated for 5 hr and then the medium was changed and the cells were incubated again for 24 hr. After that the 3-(4,5 sec-dimethylthiazol-2-yl)-2,5-diphenyl tetrazolium bromide (MTT) assay was carried out according to the method as previously reported [69].

II.2.2.5. *In vivo* DOX content in tumours

DLBs (70 µg DOX and 330 µg lipid) in 5% glucose (final volume of 200 µl) were intravenously injected and then immediately tumours were irradiated with TUS for 60 s.

Mice were sacrificed 15 min after the injection of DLBs and subsequently tumours, hearts and livers were harvested, weighed and preserved at −80°C. DOX was extracted by homogenising the tumours with a mixture of isopropanol and 1 M HCl aqueous solution (1:1 v/v) and incubated for 1 hr at 4°C. It was then centrifuged at 13,000 g for 15 min, and the supernatants were recovered for fluorescence detection (FluoroMax4, Horiba, Ltd., Kyoto, Japan). DOX standard series were prepared in non-treated tumour tissues extracts.

II.2.2.6. *In vivo* tumour inhibition and imaging

The first treatment was initiated on the 9^{th} day after tumour cell inoculation and repeated on the 11^{th} and 13^{th} days. Immediately after intravenous administration of DLBs, the tumour site was irradiated for 60 s with TUS (2 MHz; 2W/cm²; 50% Duty; 10 Hz). Tumour volume was measured every 2–3 days using the formula: (major axis×minor $axis^2$) ×0.5.

HRI nude mice (n = 3) inoculated with B16BL6 melanoma were anaesthetized and placed on an imaging pad; temperature, heart rate and breathing were continuously monitored. DUS imaging was performed as previously described [70]. Briefly, a dedicated small animal high-spatial-resolution imagining liner transducer (16 MHz; gain, 25 dB; dynamic range, 50 dB) (Vevo 2100) was used. Subsequently, DLBs were injected at a dose of 100 µl/mouse (300 µg/ml lipid) and images (460 frames) were obtained before and after injection. The data were analysed by comparing the differences in contrast enhancement signal at tumour sites. For investigating the DLBs path through the tumour vasculature, the maximum intensity persistence analysis (MIP) mode (Vevo 2100) was used.

II.2.2.7. Statistical analysis

All data were analysed as the mean ± SEM. Unpaired, the two-tailed distribution Student's t-test was applied and values of $P < 0.05$ were considered as being statistically significant.

II.2.3. Results

II.2.3.1. *In vitro* DOX uptake and MTT assay

In vitro, DOX delivery was investigated in B16BL6 cells using confocal scanning microscopy. The combination of DLBs with TUS irradiation (Fig. 17A) showed higher cellular accumulation of DOX 15 min after treatment compared with DLBs in the absence of TUS irradiation (Fig. 17B). The combination of free DOX with TUS irradiation did not give high levels of DOX (Fig. 17C).

Unloaded bubbles that has no DOX (ULBs) in combination with TUS irradiation resulted in a decrease in tumour cell viability by about 32.5%, suggesting that there were cavitation effects associated with ULBs in combination with TUS irradiation. DLBs used in the absence of TUS irradiation resulted in a decrease in cell viability of approximately 27%. In contrast, cell viabilities were significantly lower after treatment with DLBs combined with TUS irradiation than those treated with DLBs in the absence of TUS irradiation (1.5 and 3.0 μg/ml DOX) (Fig. 18).

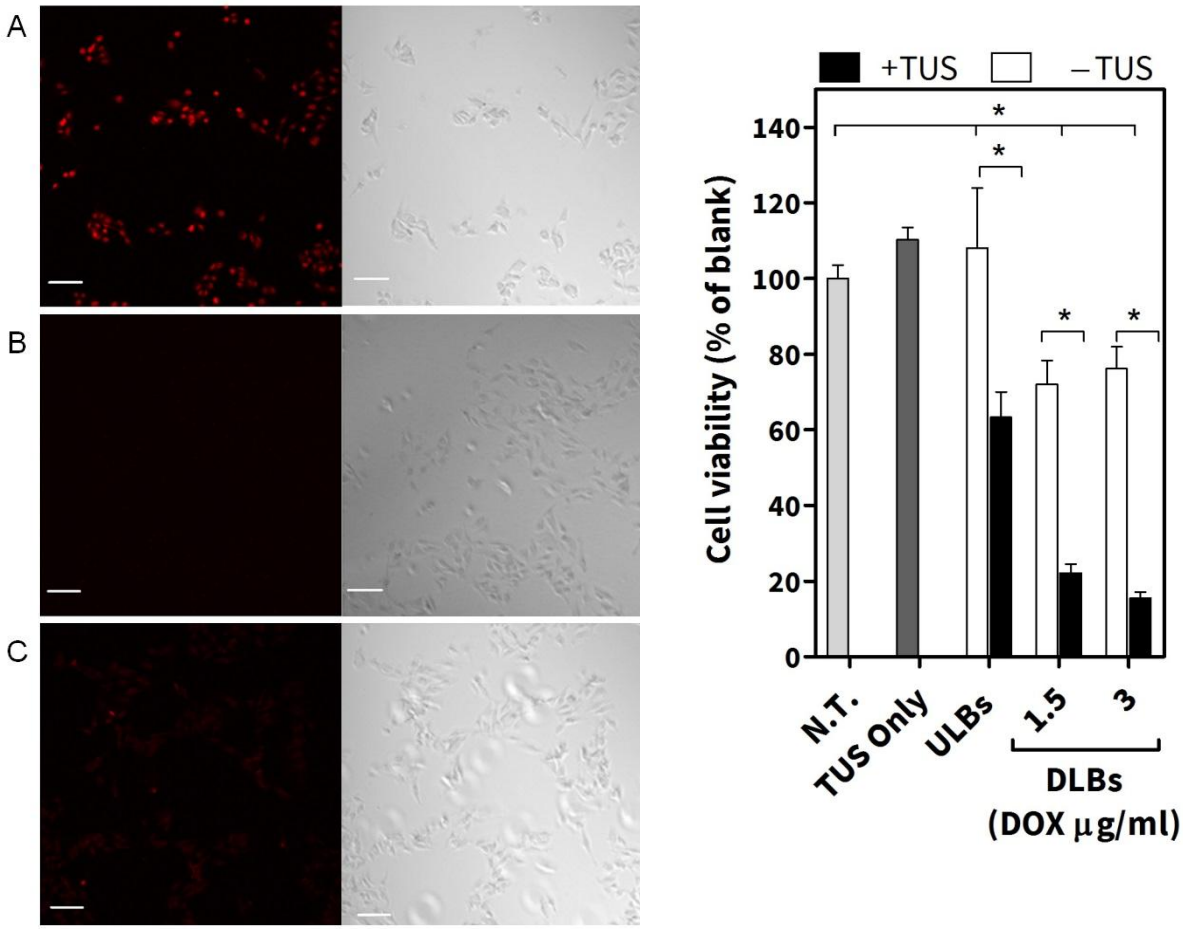

Fig. 17. Confocal laser microscopy images of B16BL6 cells having DOX with various methods. (A) DLBs in combination with TUS irradiation, (B) DLBs in the absence of TUS irradiation and (C) Free DOX in combination with TUS irradiation (scale bar, 50 μm). Cells were treated with DLBs and free DOX in combination with TUS irradiation and then incubated for 15 min prior to the analysis.

Fig. 18. The viability of B16BL6 melanoma cells after treatment with DLBs, ULBs; unloaded microbubbles (0 DOX) and TUS irradiation alone. Each bar represents the mean ± SEM of six experiments. * $P < 0.05$ versus the corresponding groups with no treatment (N.T.).

II.2.3.2. Intratumoral content of DOX in tumour bearing mice

As shown in Fig. 19, the combination of DLBs with TUS irradiation significantly enhanced the intra-tumoral DOX level (0.536 μg/g tissue) as compared with DLBs without TUS irradiation (0.100 μg/g) (Fig. 19A). Conversely, the levels of DOX in liver (Fig. 19B) and heart (Fig. 19C) did not significantly differ between the two groups.

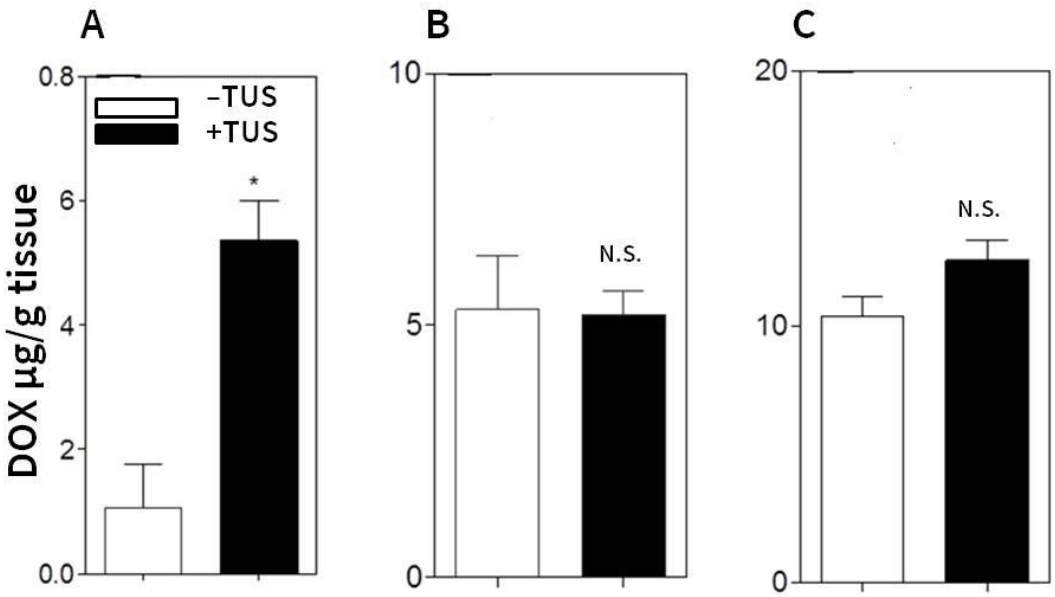

Fig. 19. DOX distribution characteristics after intravenous administration of DLBs with or without TUS irradiation in tumour bearing mice. The DOX content was measured in (A) Tumour, (B) Heart and (C) Liver. Each bar represents the mean ± SEM of five experiments. * $P < 0.05$ versus the corresponding group that received DLBs in combination with TUS irradiation.

II.2.3.3. Tumour growth inhibition and body weight change in tumour bearing mice

By day 27 after tumour inoculation, tumour volume in the control group had aggressively increased (7156 ± 1384 mm^3). The tumour volume was slightly reduced relative to the control group (4663 ± 454 mm^3) in the group of mice treated with DLBs in the absence of TUS irradiation. In contrast, the group of mice treated with DLBs in combination with TUS irradiation, showed significant reduction of tumour growth (2454 ± 175 mm^3) (Fig. 20A). Moreover, treatment with DLBs in combination with TUS irradiation did not cause any significant loss of body weight relative to the control

group (Fig. 20B).

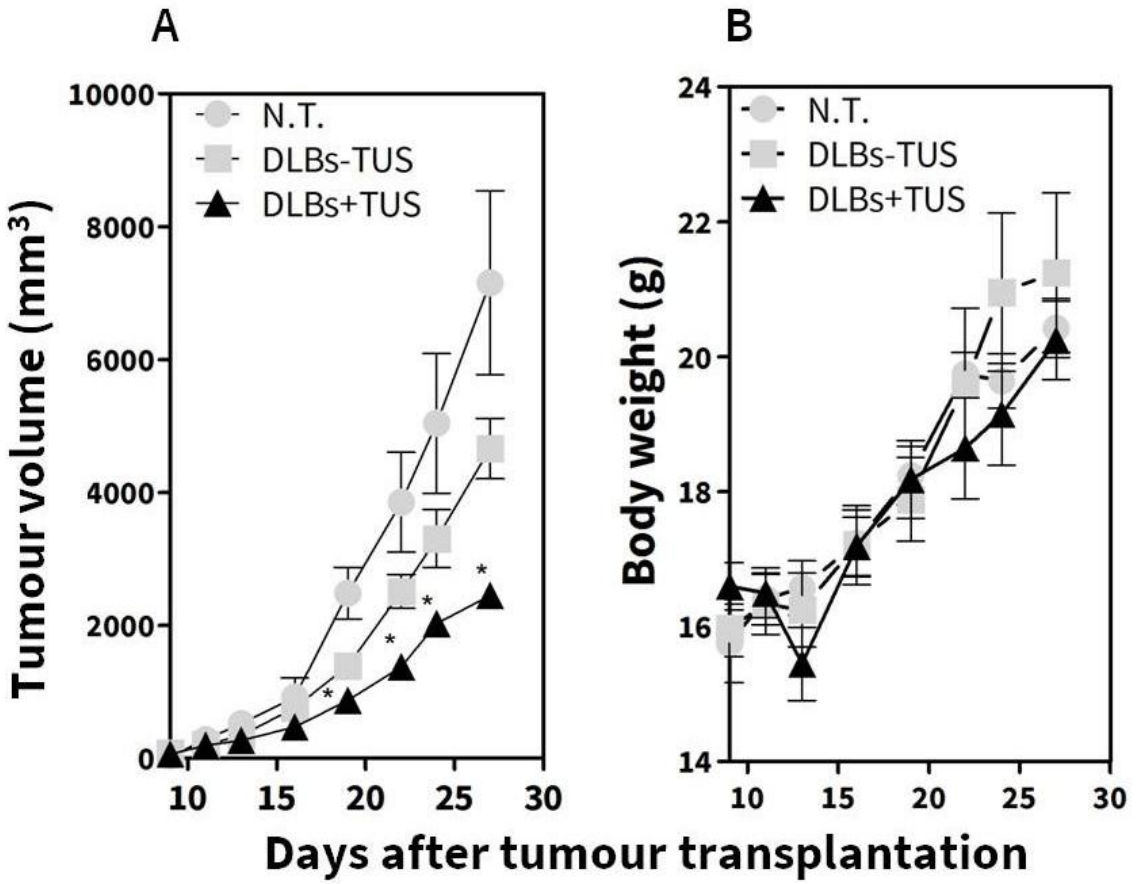

Fig. 20. Effect of DLBs administration with various methods on tumour growth and body weight change. (A). Tumour volume in mice. (B). Mouse body weight. Mice were divided into three groups: control; DLBs only; and DLBs in combination with TUS irradiation. Treatment was performed on the 9th day after tumour transplantation and was repeated on the on the 11th and 13th days. Each bar represents the mean ± SEM of 5–6 experiments. * $P < 0.05$

II.2.3.4. *In vivo* ultrasonography

After 1 min, the intensity of the contrast enhancement signal was gradually reduced (Fig. 21A). The images were analysed by plotting the mean contrast intensity in the tumour area against time after DLB injection (Fig. 21B). The half-life time of intensity decrease of DLBs was estimated to be between 2–3 min. Moreover, the maximum intensity persistence (MIP) analysis clearly revealed the distribution of DLBs in the

tumour vasculature with a clearly distinguishable contrast signal (Fig. 21C).

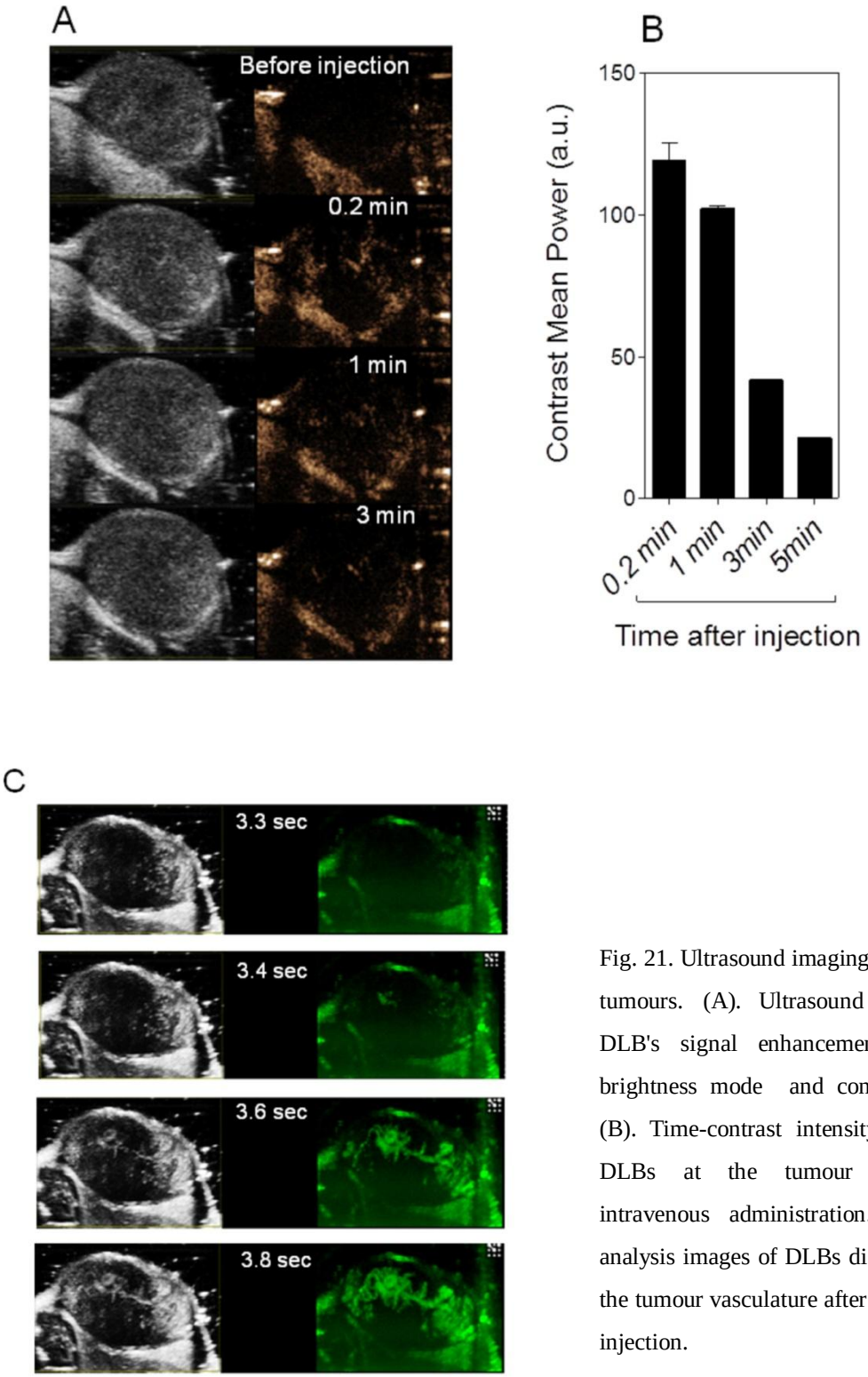

Fig. 21. Ultrasound imaging of DLBs in tumours. (A). Ultrasound images of DLB's signal enhancement in both brightness mode and contrast mode. (B). Time-contrast intensity graph for DLBs at the tumour site after intravenous administration. (C). MIP analysis images of DLBs distribution in the tumour vasculature after intravenous injection.

II.2.4. Discussion

In this section, I demonstrated that DOX uptake in cancer cells was enhanced when DLBs were combined with TUS irradiation, leading to high *in vitro* cytotoxicity and effective *in vivo* DOX delivery (Fig.17). Bubbles in combination with TUS can cause perturbation of the cell membranes and hence enhance drug permeability in a reversible process that lasts for a couple of minutes [50]. Unlike Tinkov and co-workers, I found a significant difference in doxorubicin uptake between DLBs with ultrasound compared with free doxorubicin 15 minutes after treatments [26]. This difference could be due to the experimental conditions like the DOX incubation time. It is well known that DOX is easily taken up by the cells through passive diffusion and the active transport mechanism which means that the long incubation time used by Tinkov *et al* might have lead to a substantial contribution from this way of uptake to the total drug amount [71]. Lentacker *et al* found that after 15 minutes of treating cells with free DOX, the amount of internalised DOX by the cells was much lower than those treated with bubbles loaded with DOX-liposomes [21]. Based on this, minimising the incubation time can be critical for understanding the sonoporation process when bubble cavitation occurs.

In the *in vivo* experiment, it is expected that TUS irradiation at the tumour site leads to DLB's cavitation and DOX release; consequently, the concentration of free DOX was increased in tumour but not in the heart and liver. Furthermore, DLBs in combination with TUS significantly inhibited tumour growth without any reduction in animal body weight. These results suggest that DLBs combined with TUS irradiation at the tumour site could improve treatment accuracy and safety with less systemic side effects including cardiotoxicity.

In the tumour, DOX might have been delivered primarily to the endothelial cells of

the tumour microvasculature. Subsequently, nutrition supply to the tumour would be disrupted due to necrosis caused by dead endothelial cells [72]. However, direct delivery of DOX into tumour cells might have occurred as well. It has been reported that cavitation effects can enhance drug penetration into the tumour by further "opening up" of the endothelial barrier [73].

As shown in Fig. 21, the imaging potential of DLBs was confirmed by DUS ultrasonography imaging, which revealed a high contrast enhancement signal in the tumour area in mice after DLBs administration. Moreover, I showed that the contrast mode signal from DLBs in the tumour vasculature could be clearly distinguished from the surrounding healthy tissues. Pysz *et al* have reported that *in vivo,* the ultrasound imaging signal in tumour bearing mice using MIP algorithm could be used to assess tumour vascularity [67]. That is because a correlation between the *in vivo* MIP values with microvessel density analysis was observed. Therefore, tumour angiogenesis could be monitored by evaluating the MIP analysis of DLBs distribution in the tumour vasculature.

In conclusion, DLBs will function as a theranostic carrier in both *in vitro* and *in vivo*. DLBs stability *in vivo* was enough for conducting the DUS imaging as well as for the delivery of DOX when triggered with TUS. Therefore, these results strongly support the potential use of DLBs as a vasculature probe in tumor theranostics.

Section II. 3

Investigation on the use of liquid cored ultrasound contrast agents for cancer theranostics: Systemic administration route

II.3.1.Introduction

The great trend of tumour targeting started with the discovery of the enhanced permeability retention effects (EPR). EPR effects were first reported by Matsumura and Maeda; they found that solid tumours usually have defective and impaired vasculatures unlike normal tissues [74]. Depending on this anatomical abnormality in tumours, it was found that macromolecular with a moecular weight larger than 40 kDa could preferably extravasate into tumours rather than other organs. And due to the lack of lymphatic drainage, this macromolecular can be trapped inside the tumour site [75, 76]. Since then, this mechanism has been used for passive targeting to tumours with liposomes or micelles that were loaded with anti-cancer drugs. For instance Doxil, a PEGylated liposome loaded with DOX, is used for targeting Kaposi sarcoma and other types of solid tumours [77]. Doxil has a size range of few hundred nanometres and can sustain in the circulation more than small molecular weight drugs. These characteristics were found to be critically contributing in enhancing the EPR effects in tumours [78].

Gas cored UCAs have limited ability for EPR mediated passive accumulation into the tumour. That is because of the large size of bubbles in addition to their short stability under the physiological conditions. Consequently, their access mostly is limited to neovasculature's spatial area [6, 79]. However, for inducing sufficient inhibition in tumour cells, direct delivery of cargo to cancer cells is a pre-requisite. Therefore, the design of new generation of UCAs that have the ability of passive targeting is of importance. That means that drug loaded UCAs should first extravasate into tumour bed

passively (EPR effects) and then followed by TUS irradiation after specific time for stimulating drug release nearby cancer cells. In section I 4, I showed that by utilising phospholipids and liquid PFCs, bubble precursors could be prepared. These bubbles precursor or phase shift acoustic nanodroplets (PSANDs) had an average size of 200 nm and they were stable at the physiological temperature for at least 1 hr. Moreover, droplets could effectively be shifted to bubbles by TUS irradiation *in vitro* setting. Starting from these basic *in vitro* investigations, PSANDs were expected to be useful for tumour passive targeting through EPR effects after systemic administration. Thus, (PFH)PSANDs were selected for the systematic investigations. It was reported that high boiling point PFCs can have better systemic stability *in vivo* [80, 81]. Therefore, I expected that for systemic administration, PFH with boiling point ~56 ^{O}C can achieve better *in vivo* stability.

Taking all of these into consideration, in this study, the *in vitro* stability of (PFH)PSANDs in the presence of serum was first evaluated. That was followed by testing the *in vivo* phase-shift-transition of droplets-to-bubbles after TUS irradiation. Finally, the potential of (PFH)PSANDs in tumour passive targeting was assessed in tumour bearing mice.

II.3.2. Materials and methods

II.3.2.1. Animals and tumour models

Female 6-week-old ICR mice and female 6-week-old C57BL6 mice were purchased from the Shizouka Agricultural Cooperation Association for Laboratory Animals (Shizouka, Japan). Tumour bearing mice were prepared as described in Section II 2.

II.3.2.2. *In vitro* Stability of droplets in the presence of serum

Briefly, 100 µl of (PFH) PSANDs were mixed with 500 µl PBS with 10% serum extracted from rats. Samples were placed in water bath at 37° C and 10µl sample was collected at different time points for gas chromatography (GC-MS) analysis as described in Section I 1.

II.3.2.3. *In vivo* ultrasonography imaging

ICR mice were used to perform the imaging process. In this experiment, the left carotid artery in the mouse was imaged. Doppler mode was used to determine the artery area. Droplets were injected intravenously via the tail vein (225 µg lipid /mouse with a final volume of 200 µl). Two minutes later 1000 frames of ultrasonography video was recorded. During that, two burst of TUS (at frame number 568 and frame number 783) were applied for provoking droplets phase transition into bubbles. The images were shown in linear mode and the contrast enhancement was marked with a green colour.

II.3.2.4. *In vivo* bio-distribution of droplets

(PFH)PSANDs was injected intravenously (400 µg lipid / mouse in final volume of 250 µl) via tail vein of mice. After 3, 15, and 60 min blood, tumour, and other organs were collected. Samples were moved into GC vials, capped, and kept at 4 °C for further analysis by GC-MS system as described in Section I 1. The retention time of PFH was first confirmed by using only crude PFH. Data are presented in AUC of PFH peak at retention time of 10.9 min. The dose percentage was then calculated by dividing AUC of samples by AUC of the initial dose. The results were then normalised by the total blood volume in mice (assumed to be 1.5 ml) in the case of blood samples and by weight in the case of tissues.

II.3.3. Results

II.3.3.1. *In vitro* PSANDs stability in serum

PSANDs were challenged in the presence of serum for the time course of 120 min. The level of PFH was more and less unchanged through incubation time of 90 min. At 120 min some PFH was leaked but still over 50 % was packed in the droplets (Fig. 22).

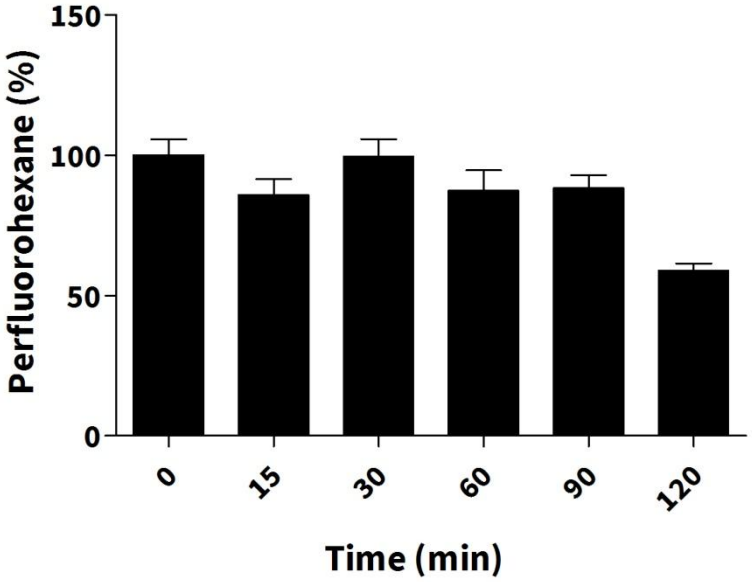

Fig. 22. *In vitro* PSANDs stability in the presence of serum. PFH nanodroplets were incubated in 10% serum in PBS at 37 C, and at specific time points samples were collected for GC-MS analysis of PFH. n = 3; mean ± SEM

II.3.3.2. *In vivo* ultrasonography imaging

For identifying the location of left carotid artery, colour doppler mode and Pulsed Wave doppler mode (PW) was used. Both left carotid artery and left internal jugular veins were clearly detected depending on the blood velocity direction. The red coloured spots mean that the blood movement is towards the DUS probe (arterial blood flow), while the blue coloured spots mean that blood was moving away from DUS probe (venous blood flow). This was supported also with PW mode that showed positive

blood velocity values in the previous location. (PFH)PSANDs were then intravenously administrated and after 2 min ultrasonography imaging was performed (Fig. 23A). Immediately after first TUS irradiation, specific contrast enhancement was noticed in the carotid artery area only. Similar contrast enhancement was noticed as well after the second TUS irradiation (Fig. 23B). Contrast enhancement signal was sustained for a few hundred frames and ultimately decreased to the background levels (Fig. 23C).

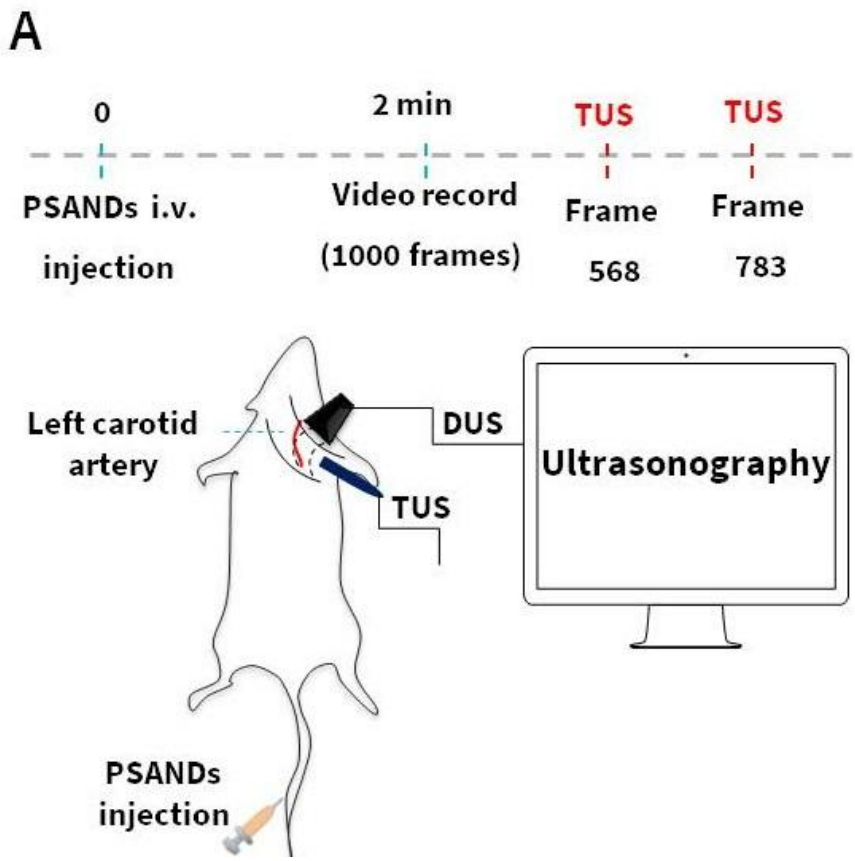

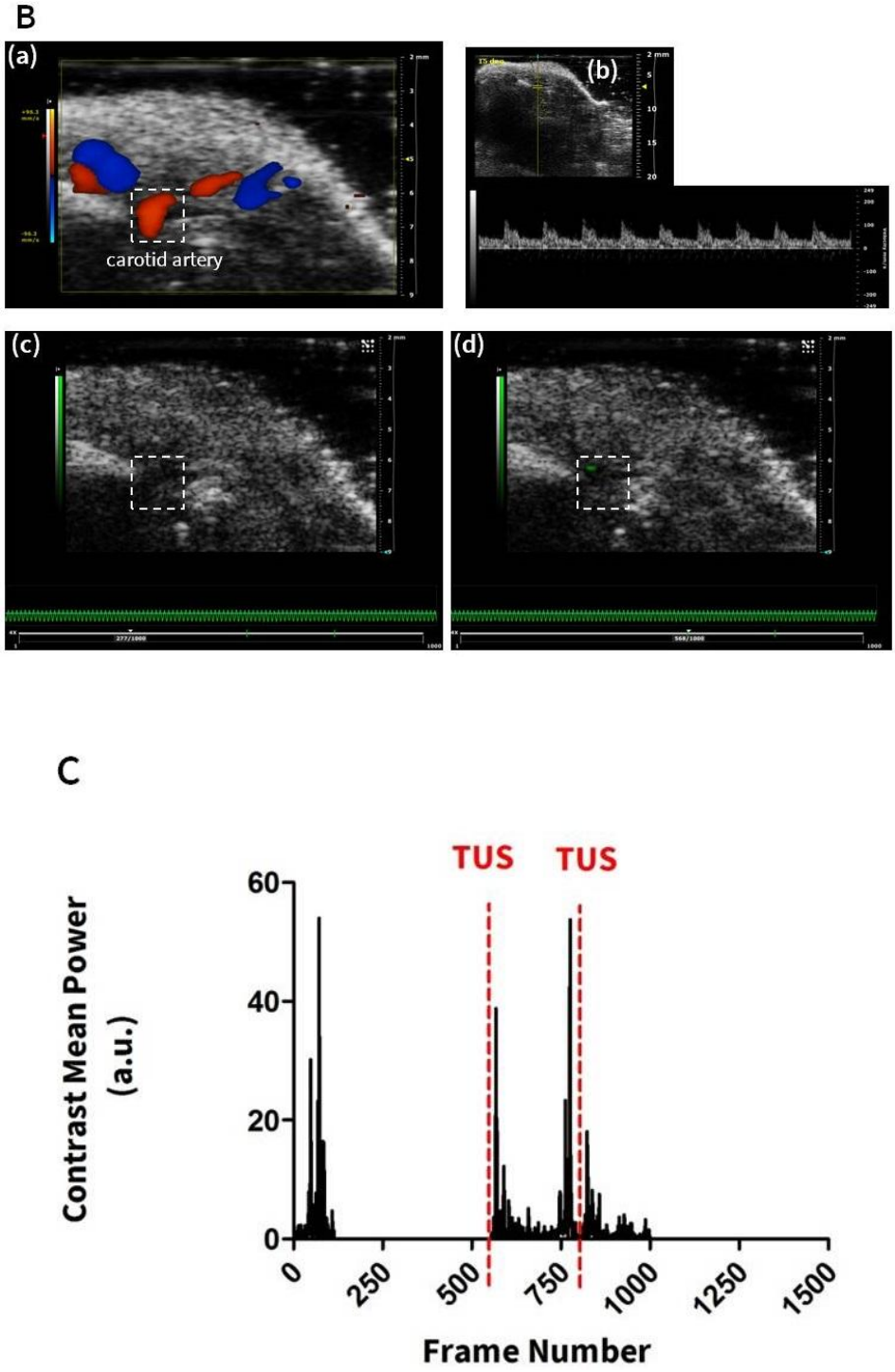

Fig. 23. *In vivo* ultrasonography in the carotid artery of mouse. (A). The study protocol and experimental setting. (B). ultrasonography images: a). Colour Doppler mode. b). PW Doppler. c). Brightness mode before TUS. d). Brightness mode after TUS immediately. (C). The contrast enhancement of PSANDs before and after TUS irradiation.

II.3.3.3. *In vivo* bio-distribution of PFH in tumour bearing mice

For evaluating the passive accumulation of (PFH)PSANDs in the tumour, PFH was quantified by GC-MS. PFH was retained in the blood pools for almost 15 min (33.9% of ID/ 1.5 ml blood) as well as in tumour (1.50% of ID/ g tissue). However, after 15 min PFH levels in both blood and tumour was gradually reduced (Fig 24A and B). On the other hand, at 60 min most of PFH was taken up by spleen, liver, and lung (104.5%, 3.68%, and 2.99%, respectively of ID/ g tissue) (Fig. 24C). Moreover, the tissue/blood ratio of all organs including tumour was notably increased after 60 min (Fig. 24D).

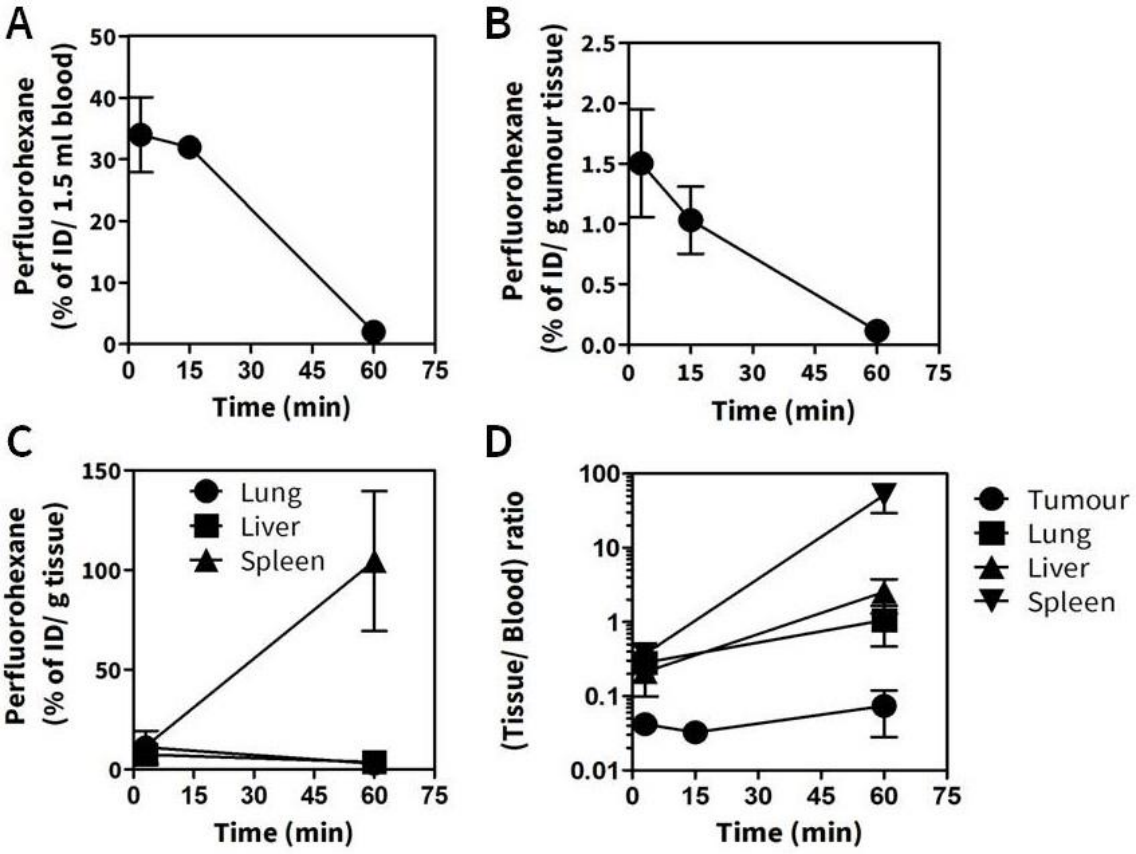

Fig.24. *In vivo* PFH bio-distribution in tumour bearing mice**.** (A) Blood (B) Tumour (C) Lung, Liver, and Spleen (D) The tissue/ blood ratio of PFH at 3 and 60 min after administration. n = 3-4 mice; mean ± SEM

II.3.4. Discussion

For more effective theranostic outcomes in cancer, tumour passive targeting is obviously an important approach. Gas cored UCAs, however, are characterised by large sizes and poor *in vivo* stability that limits their use in EPR mediated tumour passive targeting. To overcome these limitations, in Section I 4, I prepared PSANDs that were made of liquid PFCs and phospholipids. PSANDs had a smaller size around 200 nm and good *in vitro* stability under physiological conditions. Moreover, PSANDs were non-echogenic without TUS. By irradiating PSANDs with TUS, bubbles were formed and contrast enhancement was detected *in vitro* via ultrasonography imaging. In the current study, I further investigated the potential of (PFH)PSANDs, mainly, *in vivo*. This included two aspects: first, the possibility of inducing acoustic droplet vaporisation (ADV) *in vivo* assisted by both therapeutic and diagnostic US modalities, second, the assessment of tumour passive targeting by (PFH)PSANDs through EPR effects.

Before starting the *in vivo* investigation I conducted one more *in vitro* experiment. In this test, I evaluated PFH leakage in the presence of serum. This is important because serum components usually are one of the main factors that are responsible for destabilising phospholipids based carriers such as liposomes [82]. The results showed that almost 100 % of PFH was retained in droplets during 90 min in the presence of rat serum and at 37 ^{O}C. This result indicated that (PFH)PSANDs can possibly resist the circulation conditions after systemic administration.

TUS irradiation could clearly induce ADV; as specific contrast enhancement was generated in the carotid artery area. These results indicated that (PFH) PSANDs were capable in undergoing the physical shift from droplets (PFH liquid) to bubbles (PFH gas) *in vivo* thus contrast signal was detected. Also, these results were comparable to the

reported results with PFPn droplets in which droplets were activated with TUS and observed by ultrasonography 1 min after administration [83].

At the beginning of ultrasonography imaging, some unspecific contrast enhancement was detected between frame 0 and frame 114, but soon this signal was reduced to the baseline levels. A possible reason can be due to the pre-existence of some gas bubbles in the PBS buffer that was pre-mixed with droplets before administration. Therefore, these gas bubbles could generate some contrast signal, which, however, soon reduced possibly due to the dissipation of bubbles from circulation.

For evaluating the biodistribution of (PFH)PSANDs *in vivo*, I quantified the amount of PFH in tumour bearing mice. Many *in vivo* studies have been performed with droplets that made with (PFPn) but not much is available about the fate of PFH *in vivo* after systemic administration [84, 85]. For example, Shiraishi et al showed that droplets made with block copolymer surfactant and PFPn could not sustain much *in vivo* in the blood (~10% of ID remaining after 10 min) [86]. In my results, PFH could be sustained in blood at least for 15 min. And eventually; PFH was mostly disappeared at 60 min. That was opposed by the great increase of PFH uptake by spleen in the first rank followed by liver and lunge, respectively. Several reports indicated also the tendency of PFC droplets to accumulate more in spleen rather than the liver. The mechanism was not clearly addressed, but it is assumed that phagocytosis by mononuclear cells in both liver and spleen is responsible for that [87]. On the other hand, PFH in the tumour was reduced by almost 33% at 15 min (assuming PFH values at 3 min as 100 %). And then a great decrease was noticed at 60 min. However, the tissue/blood ratio showed some increase in the tumour uptake of PFH at 60 min. Theoretical calculation of the number of droplets in the tumour tissues showed that around 4.6×10^9 droplets per a tumour

(average weight 0.654 g and assuming droplets with a diameter of 200 nm) at 15 min. Therefore, it is possible that the decrease of PFH in the tumour can be due to the *in situ* PFH clearance after droplets destabilisation due to coalesces in the tumour that led to PFH leakage. It was seen that droplets in spleen and liver can aggregate in clusters bigger than the initial droplets size. Consequently, coalescence occurs leading to the leakage of PFCs. After that, PFCs are released back to the blood and finally, lipoprotein facilitates their transport before expiration via the lung [88]. Therefore, it could be that similar scenario might occur with (PFH)PSANDs in the tumour. In this context, Fan et al also reported similar observation with droplets (~300 nm) that were made with egg phosphatidylcholine and perfluoro-15-crown-5-ether [81]. Another important observation was related to the PFH accumulation in lungs. Reducing PFC accumulation in the lung is important for maintaining suitable gas exchange, otherwise, respiratory distress might occur and consequently death [89]. In my results, a dose of 2.8×10^{13} droplets/ kg (mouse weight ~25 g) was used, and PFH accumulation in the lung was little compared to that in spleen and liver which indicated that (PFH)PSANDs size was small enough so that no pulmonary trapping has taken place. Zhang et al reported that administrating PFP droplets (~2 μm) could lead to respiratory distress in a canine model possibly due to the large size of droplets that impaired the lung function in maintaining suitable gas exchange [90].

In conclusion, (PFH)PSANDs had better *in viv*o stability compared to gas cored UCAs. Also, further investigations are needed to confirm more the passive accumulation behavior of (PFH)PSANDs. Overall, these results are ought to add valuable information related to the rational design of (PFH)PSANDs and their potential as theranostic carrier mainly after systemic administration.

Section II. 4

Investigation on the use of liquid cored ultrasound contrast agents for cancer theranostics: Intratumoral route

II.4.1.Introduction

Hyperthermia is one of the well known methods in cancer therapy. In this approach temperature increase between 40-44^{O}C is found to cause cytotoxic effects in the tumour. Also, cancer cells susceptibility toward other types of therapy (e.g., chemotherapy and radiotherapy) was increased [91]. The mechanism beyond that was related mainly to protein denaturation in addition to the changes in the cellular level (e.g., damage in the skeleton, the membrane, and DNA synthesis).

High intensity focused ultrasound (HIFU) is a type of therapeutic US that mainly used for thermal tumour ablation. This uses an external transducer that can generate a focal intensity of few thousand W/cm^2. The ultrasound beam passes through the intact skin and is concentrated in one region, deep inside the organ. The acoustic absorption in the focal volume leads to temperature elevation which ranges from 60 to 95 °C. This temperature elevation causes protein denaturation and coagulative necrosis in the tissue [92]. HIFU tumour ablation therapy has recently become more common and has been recognised clinically for several tumours types, including those of the prostate, pancreas, liver and breast [93, 94]. However, HIFU has some drawbacks that limit its use. For example, skin damage might occur during therapy. Also, in some sort of tumours such as skin superficial tumour (e.g., melanoma) HIFU cannot be used. That is because HIFU system is mainly designed for deep solid tumours but not for superficial tumour hence adjusting the focal point of HIFU system is technically hard [95]. In this case, unfocused TUS can be more functional and skin superficial area can easily be irradiate

with TUS. The intensity of US should be enough to induce suitable thermal effects in tumour area (~ 40^{O}C) but not too much high so that no skin burns occur in the tumour rim. In such a controversial condition, addressing a new method for overcoming the previous limitations is needed.

The co-treatment of gas cored bubbles with TUS accelerates the efficacy of TUS irradiation due to their strong cavitation capability [96, 97]. It has been reported that the co-treatment of MBs with HIFU increases heat generation and thus the necrosis rate in ablated tissue comparing to HIFU alone [98]. Moreover, Farny et al. observed a correlation between cavitation power and heat generation. It was suggested that inertial cavitation could lead to temperature elevation [99]. Interestingly, PSANDs in combination with TUS were found to accelerate heat generation too, due to bubble cavitation, and the energy needed for forming a lesion was significantly decreased [100].

For increasing the treatment efficacy and decreasing the systemic side effects, tumour site-specific targeting is preferable. That can be achieved by the direct injection of the therapeutic compounds into tumour [101]. This approach is much possible especially in the case of skin superficial tumours. Moreover, the direct injection of lipid based-emulsion (water-in-oil) loaded with anti-cancer drugs was found to be enhancing the transport of anti-cancer drug to the lymphatics [102]. Also, It was reported that after intratumoral injection of lipid-based emulsions, only droplets with size around 250 nm could be retained in the tumour tissue for a longer time [103]. In section I 4, I showed the facile preparation of phospholipid-based PSANDs. Droplets that made with perfluropentane (PFPn)PSANDs had an average size between 200-300 nm and they were sensitive toward low-intensity TUS (~ 2W/cm^2). These droplets have the basic

emulsion characteristics that might enhance their retention inside the tumour after intratumoral injection. Additionally, the irradiation of a low-intensity unfocused TUS can induce thermal or histotripsy damage in the tumour.

In this study, the use of (PFPn)PSANDs in tumour hyperthermia therapy after direct intratumoral injection was investigated in B16BL6 tumour bearing mice. Droplets were intratumorally injected and that was followed by low-intensity TUS irradiation on the tumour area. Both thermal analysis and tumour inhibition studies were conducted accordingly.

II.4.2.Material and methods

II.4.2.1. Animals and tumour models

Female 6-week-old C57BL6 mice were purchased from the Shizouka Agricultural Cooperation Association for Laboratory Animals (Shizouka, Japan). Tumour models were prepared as described in Section II 2.

II.4.2.2. Temperature elevation in tumour site

Temperature elevation was assessed by thermography monitoring system (NEC Avio Infrared Technology Co., Tokyo, Japan). Briefly, 25µl of droplets or PBS was injected in the centre of the tumour. The injection needle was kept at the injection site and thermographs were then taken. Five minutes after injection, TUS irradiation was applied (1MHz, 2W/cm2, 50 % duty, 10Hz) for 2 min. Thirty seconds after that, thermographs were obtained again.

II.4.2.3. Tumour inhibition study

Mice were divided into three groups (n=4-5 each); no treatment, PBS with TUS, and PFPn(PSANDs) with TUS. The first treatment was considered 0 days. Similarly,

25µl of droplets or PBS was injected in the centre of the tumour. The injection needle was kept at the injection site and 5 min after injection, TUS irradiation was applied (1MHz, 2W/cm2, 50 % duty, 10Hz) for 2 min. Tumour volume was measured every 2–3 days using the formula: (major axis×minor axis^2) ×0.5.

II.4.3. Results

Thermography images were used to show the changes in temperature after TUS irradiation in the tumour sites. In mice treated with PBS with TUS, there was no increas in temperature after TUS irradiation (Fig. 25A). On the other hand, a distinguished temperature elevation was seen in tumours treated with PFPn (PSANDs) (Fig. 25B). In the tumour inhibition study, 8 days after tumour transplantation tumour volume in the no treatment group had quickly increased (4020.4 ± 1409 mm^3).

The tumour volume was slightly reduced relative to the no treatment group (3273.5 ± 822 mm^3) in the group of mice treated with PBS with TUS irradiation. In contrast, in the group of mice treated with PFPn(PSANDs) in combination with TUS irradiation, there was significant reduction of tumour volume (2314.8 ± 925 mm^3) (Fig. 26A). Moreover, treatment with PFPn (PSANDs) in combination with TUS irradiation did not cause any significant loss of body weight relative to the control group (Fig. 26B).

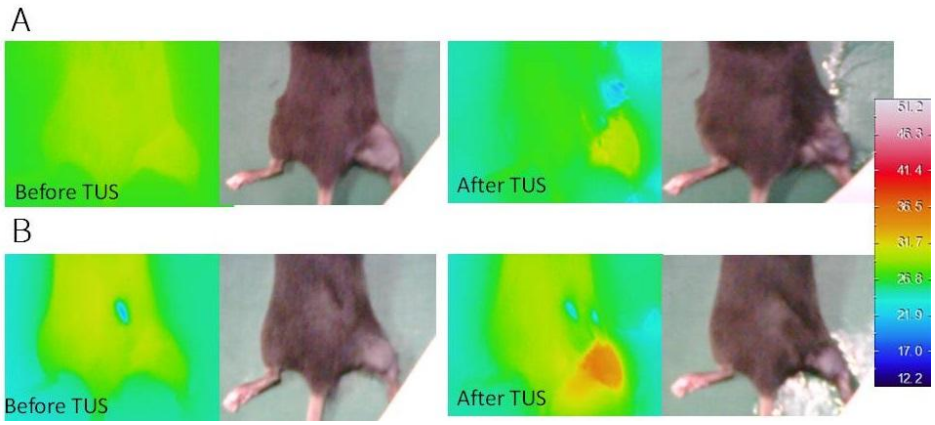

Fig. 25. Thermographic analysis (A). Mice treated with PBS. (B). Mice treated with (PFPn)PSANDs. Mice were divided into two groups: with PBS and with (PFPn) PSANDs TUS irradiation.

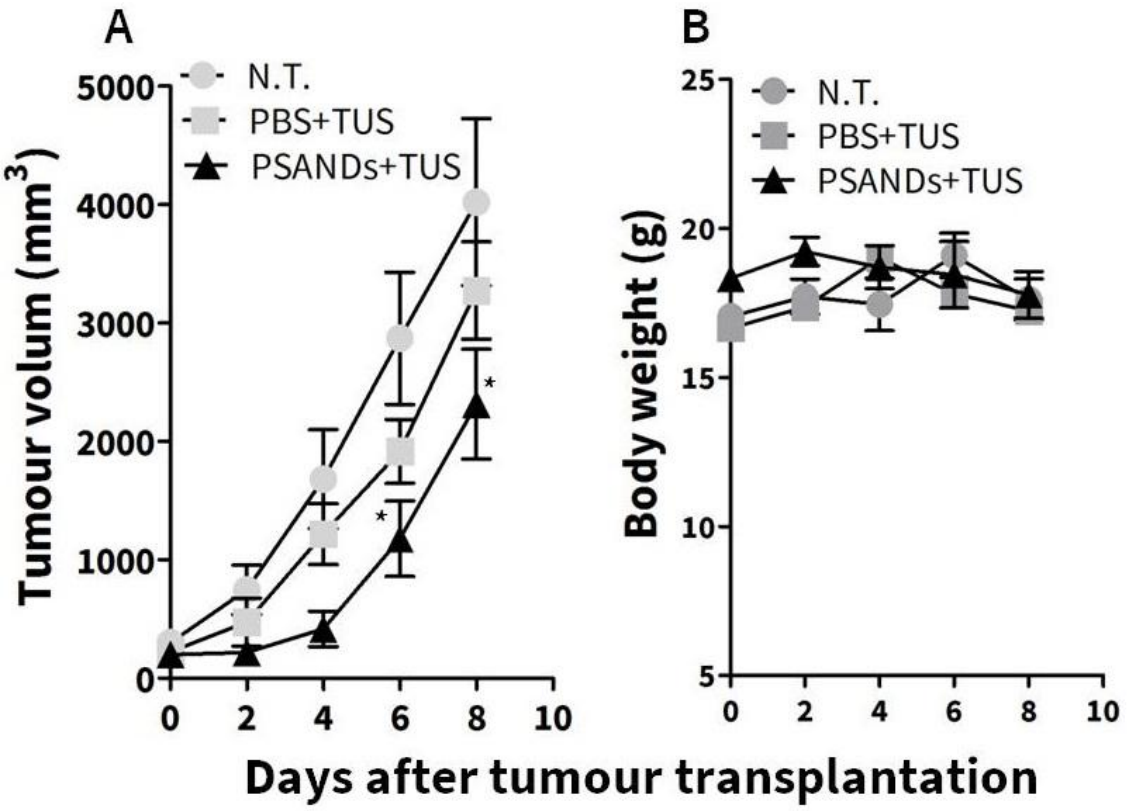

Fig. 26. Effect of (PFPn)PSAND administration on tumour growth and body weight. (A). Tumour volume in mice. (B). Mouse body weight. Mice were divided into three groups: No treatment (N.T); PBS in combination with TUS; and (PFPn)PSANDs in combination with TUS irradiation. Treatment was performed on the 10^{th} day after tumour transplantation. Each bar represents the mean ± SEM of 4 experiments. * $P < 0.05$

II.4.4. Discussion

The use of HIFU in tumour thermal ablation is already proved to be useful clinically in several types of solid tumours. However, this is limited in the case of skin superficial tumour. An alternative for that can be addressed through the co-treatment of UCAs with unfocused low-intensity TUS. Under the acoustic pressure of TUS wave, UCAs can undergo stable or inertial cavitation. Cavitation in the injection site can then

induce thermal effects or histotripsy effects leading to the denaturation of tumour cells without causing excessive heat in the surrounded healthy tissues. The process can be performed by first, the direct intra-tumoural injection of UCAs and second, by the irradiation with unfocused low-intensity TUS.

In this section, I showed for the first time-according to my knowledge- that PSANDs can induce thermal elevation effects after the irradiation with low-intensity TUS on the tumour site. The temperature increase was noticed only in the tumour area, particularly in the right limb. TUS irradiation with PBS only made no changes in temperature indicated that the bubbles cavitation after droplet vaporisation could mainly contribute in increasing the temperature. Moreover, PSANDs in combination with TUS significantly inhibited tumour growth without any reduction in animal body weight.

This antitumour effect can be a consequence of the temperature increase after the treatment. Some studies showed that PSANDs could cause mechanical histotripsy damage after droplets vaporisation [104, 105, 106]. Therefore, it could be that the cavitation effects of bubbles have contributed in inducing further damage in tumour via mechanical damage effects too.

Overall, (PFPn)PSANDs in combination with unfocused low-intensity TUS have the potential to be further used in tumour hyperthermia therapy. The theranostic characteristics of these droplets will ease the treatment procedures; as droplets phase shift to bubbles can be monitored by ultrasonography. Moreover, loading (PFPn)PSANDs with some anti-cancer drugs (e.g., doxorubicin) can enhance more tumour reduction as it was reported that the cytotoxic effects of some anti-cancer drugs could be increased when theses drugs were combined with hyperthermia treatment [91]. Another important future aspect of this research is the possibility of harnessing the

tumour immunity. It was reported that low-pressure amplitude focused US (FUS) in combination with conventional bubbles such as Sonovue® have induced antitumour immunity in mice. After treatment, tumour infiltrated $CD8^+$ and $CD4^+$ were significantly increased and an up-regulation in HSP expression levels in the tumour was also noticed [107]. Suzuki et al also reported that an intratumoral injection of bubbles in combination with the low-intensity US in colon 26 tumour bearing mice, led to a significant increase in the temperature in the tumour. Additionally, extensive necrosis was induced and tumour growth was inhibited. The *in vivo* depletion of CD8+ cells completely blocked the effect of bubbles with TUS on tumour suppression, indicating that CD8+cells are involved in the tumour inhibition mechanism after treatment involving bubbles and TUS [108]. For that, it might be possible that the (PFPn) PSANDs in combination with TUS can also cause similar effects and subsequently induce tumour immunity.

Summary

In this thesis, I have demonstrated that the theranostic characteristics of UCAs can be optimised by including three critical factors. First, the utilisation of phospholipids as shell materials for UCAs. Second, the employment of PFCs as core material in UCAs. Third, the selection of suitable methods for producing theranostic UCAs. Further findings and applications are summarised as follows:

I. Formulation and evaluation of nano- and micro-sized phospholipids-based theranostic ultrasound contrast agents

A type of UCAs was developed by using mechanical agitation of lipids dispersion in the presence of perfluoropropane gas (PFP). The focus was on improving the size distribution and stability. Mechanically formed bubbles (MFBs) were composed of the zwitterionic phospholipid distearoylphosphatidyl choline (DSPC) with a portion of polyethylene glycol (PEG) engraftments. MFBs with PFP had a smaller size (~ 400 nm) compared to those made with perfluorobutane or nitrogen gases. Also, MFBs with PFP were found to be stable with uniform size for 24 hr at room temperature (RT) and at 4 °C bubbles could be preserved for 90 hr. By using a similar method, doxorubicin loaded bubbles (DLBs) were also prepared. The DLBs were prepared by mechanical agitation of phospholipid dispersion in the presence of PFP gas. The anionic phospholipid distearoylphosphatidyl glycerol (DSPG) was selected to bind doxorubicin to the bubbles by electrostatic interaction. Drug loading was ≥92% and bubbles had an average size of about 1 μm. The PFP was retained in the bubbles at least 30 min at RT. *In vitro* ultrasonography also showed that DLBs have high signal even after 10 min and when TUS irradiation was applied most of the bubbles were destroyed. This indicated that

DLBs were presumably destroyed due to cavitations effects. Phase shift acoustic nanodroplets (PSANDs) were also prepared by using a similar phospholipid composition as in the MFBs. The PSANDs were prepared in a two step process that consisted of mixing liposomes with liquid perfluoropentane (PFPn) or perfluorohexane (PFH) followed by bath sonication. PSANDs had average size of around 200 nm. PFH/ PFPn leakage was then tested *in vitro* at 37 °C. PFH/ PFPn were retained in PSANDs at least for 1 hr. The PSANDs could be turned from liquid to gas by TUS irradiation. The extent of the phase shift depended more on the US frequency than the intensity. Maximum contrast enhancement was achieved with TUS intensity about 2 W/cm^2 for (PFPn) PSANDs, and 5 W/cm^2 for (PFH)PSANDs.

These results suggest that UCAs with proper size and high drug loading can be prepared with fairly simple means. Therefore, these UCAs can be easily and effectively be used in the field of drug delivery and cancer theranostic.

II. Application of phospholipid-based ultrasound contrast agents for gene delivery and cancer theranostics

Based on the findings presented in Chapter I, two main applications were decided. The first application was employment of MFBs for gene transfection. MFBs were mixed with plasmid DNA and intravenously injected into mice followed by TUS irradiation on the left limb muscles. The gene expression was significantly higher than that in the mice treated with plasmid DNA and TUS only. Moreover, aged MFBs that left for 24 hr at RT or at 4 ℃ for several days were found to still be functional in enhancing the gene expression in mice limb muscles. The second application was the utilisation of the DLBs as a theranostic agent in tumour bearing mice. The inhibitory

effect on the proliferation of murine B16BL6 melanoma cells *in vitro* was enhanced using a combination of TUS irradiation and DLBs compared to that with only DLBs treatment. Moreover, *in vivo*, DLBs in combination with TUS significantly inhibited the growth of B16BL6 melanoma tumour in mice. Additionally, ultrasonography showed high contrast enhancement of the DLBs in the tumour vasculature. Also, I evaluated the stability of (PFH)PSANDs in mice after systematic admistiration in tumour bearing mice. Gas chromatography analysis showed that PFH can be sustained in circulation as well as in tumour for 15 min after intravenous injection. Moreover, the ultrasonography imaging in mouse carotid artery indicated that droplets could shift to bubbles after TUS irradiation leading to a contrast signal enhancement at the imaging site. Finally, the direct intratumoral inection of (PFPn)PSANDs followed by low-intensity TUS led to temperature increase in the tumour site. And subsequently, the tumour volume was significantly reduced possibly due to both mechanical and thermal effects generated form PSANDs cavitation. These results indicated the possibility of using PSANDs in both systemic and loacal (intratumoral) routes; thus more effective theranostic outcomes can be achieved.

In conclusion, this research is one of the first attempts in highlighting the theranostic potential of UCAs toward more advanced biomedical applications. Accordingly, I have developed several methods for producing different theranostic UCAs starting with phospholipids and (gas/liquid) PFCs. These UCAs have been tested *in vitro* and *in vivo* and have been shown to be effective as therapeutic and diagnostic agents in applications like gene delivery and cancer treatment.

Acknowledgment

The author would like to express his sincere gratitude to Professor Mitsuru Hashida for his support throughout the many years of the PhD course, keeping me going when times were tough, asking insightful questions, and offering invaluable advice.

The author also expresses his thanks to Associate Professor Fumiyoshi Yamashita and Lecturer Yuriko Higuchi for their useful discussions.

The author would like to deeply thanks Professor Kazuo Maruyama (Teikyo University, Faculty of Pharma Sciences, Tokyo), Associate Professor Ryo Suzuki (Teikyo University, Faculty of Pharma Sciences, Tokyo), Research Associate Johan Unga (Teikyo University, Faculty of Pharma Sciences, Tokyo), and Research Associate Yusuke Oda (Teikyo University, Faculty of Pharma Sciences, Tokyo) for their kind support and advice concerning ultrsonography imaging and other related research.

The author expresses his great thanks to Professor Shigeru Kawakami (Nagasaki University, Graduate School of Biomedical Sciences, Nagasaki) for the useful advice and the valuable discussions.

The author would like to thank his laboratory mates and the secretaries in the Department of Drug Delivery Research for their kind support.

The author would like to express his thanks to his friends and family for their warm support in hard times.

Finally, the author wants to express his love and gratitude to his beloved parents and siblings; because without their support none of this would have been possible.

References

[1] T. Faez, M. Emmer, K. Kooiman, M. Versluis, A.F.W. van der Steen, N. de Jong, 20 Years of ultrasound contrast agent modeling, Ieee Trans. Ultrason. Ferroelectr. Freq. Control. 60 (2013) 7–20.

[2] E.C. Unger, T. Porter, W. Culp, R. Labell, T. Matsunaga, R. Zutshi, Therapeutic applications of lipid-coated microbubbles, Adv. Drug Deliv. Rev. 56 (2004) 1291–1314.

[3] R. Suzuki, T. Takizawa, Y. Negishi, N. Utoguchi, K. Maruyama, Effective gene delivery with novel liposomal bubbles and ultrasonic destruction technology., Int. J. Pharm. 354 (2008) 49–55.

[4] K. Un, S. Kawakami, M. Yoshida, Y. Higuchi, R. Suzuki, K. Maruyama, F. Yamashita, M. Hashida, The elucidation of gene transferring mechanism by ultrasound-responsive unmodified and mannose-modified lipoplexes., Biomaterials. 32 (2011) 4659–4669.

[5] Y. Wang, X. Li, Y. Zhou, P. Huang, Y. Xu, Preparation of nanobubbles for ultrasound imaging and intracelluar drug delivery, Int. J. Pharm. 384 (2010) 148–153.

[6] S. Qin, C.F. Caskey, K.W. Ferrara, Ultrasound contrast microbubbles in imaging and therapy: physical principles and engineering., Phys. Med. Biol. 54 (2009) R27–R57.

[7] J.R. Lindner, J. Song, F. Xu, A.L. Klibanov, K. Singbartl, K. Ley, S. Kaul, Noninvasive ultrasound imaging of inflammation using microbubbles targeted to activated leukocytes., Circulation. 102 (2000) 2745–2750.

[8] M.L. De Temmerman, H. Dewitte, R.E. Vandenbroucke, B. Lucas, C. Libert, J. Demeester, S.C. De Smedt, I. Lentacker, J. Rejman, MRNA-Lipoplex loaded microbubble contrast agents for ultrasound-assisted transfection of dendritic cells, Biomaterials. 32 (2011) 9128–9135.

[9] Y. Oda, R. Suzuki, S. Otake, N. Nishiie, K. Hirata, R. Koshima, T. Nomura, N. Utoguchi, N. Kudo, K. Tachibana, K. Maruyama, Prophylactic immunization with Bubble liposomes and ultrasound-treated dendritic cells provided a four-fold decrease in the frequency of melanoma lung metastasis, J. Control. Release. 160 (2012) 362–366.

[10] E. Stride, M. Edirisinghe, Novel microbubble preparation technologies, Soft Matter. 4 (2008) 2350–2359.

[11] Y. Oda, R. Suzuki, T. Mori, H. Takahashi, H. Natsugari, D. Omata, J. Unga, H. Uruga, M. Sugii, S. Kawakami, Y. Higuchi, F. Yamashita, M. Hashida, K. Maruyama, Development of fluorous lipid-based nanobubbles for efficiently containing perfluoropropane., Int. J. Pharm. 487 (2015) 64–71.

[12] M. Lee, E.Y. Lee, D. Lee, B.J. Park, Stabilization and fabrication of microbubbles: Applications for medical purposes and functional materials, Soft Matter. 11 (2015) 2067–2079.

[13] R. Shih, A.P. Lee, Post-formation shrinkage and stabilization of microfluidic bubbles in lipid solution., Langmuir. 32 (2016) 1939–46.

[14] C. Szíjjártó, S. Rossi, G. Waton, M.P. Krafft, Effects of perfluorocarbon gases on the size and stability characteristics of phospholipid-coated microbubbles: Osmotic effect versus interfacial film stabilization, Langmuir. 28 (2012) 1182–1189.

[15] S. Garg, A.A. Thomas, M.A. Borden, The effect of lipid monolayer in-plane rigidity on invivo microbubble circulation persistence, Biomaterials. 34 (2013) 6862–6870.

[16] J.J. Kwan, M.A. Borden, Lipid monolayer collapse and microbubble stability., Adv. Colloid Interface Sci. 183-184 (2012) 82–99.

[17] T.-H. Chou, I.-M. Chu, Behavior of DSPC/DSPE-PEG2000 mixed monolayers at the air/water interface, Colloids Surfaces A Physicochem. Eng. Asp. 211 (2002) 267–274.

[18] T.A.M. Rovers, G. Sala, E. van der Linden, M.B.J. Meinders, Effect of temperature and pressure on the stability of protein microbubbles., ACS Appl. Mater. Interfaces. 8 (2016) 333–40.

[19] O. Tacar, P. Sriamornsak, C.R. Dass, Doxorubicin: An update on anticancer molecular action, toxicity and novel drug delivery systems, J. Pharm. Pharmacol. 65 (2013) 157–170.

[20] Y. Ueno, S. Sonoda, R. Suzuki, M. Yokouchi, Y. Kawasoe, K. Tachibana, K. Maruyama, T. Sakamoto, S. Komiya, Combination of ultrasound and bubble liposome enhance the effect of doxorubicin and inhibit murine osteosarcoma growth., Cancer Biol. Ther. 12 (2011) 270–277.

[21] I. Lentacker, B. Geers, J. Demeester, S.C. De Smedt, N.N. Sanders, Design and evaluation of doxorubicin-containing microbubbles for ultrasound-triggered doxorubicin delivery: Cytotoxicity and mechanisms involved., Mol. Ther. 18 (2010) 101–108.

[22] S. Tinkov, C. Coester, S. Serba, N.A. Geis, H.A. Katus, G. Winter, R. Bekeredjian, New doxorubicin-loaded phospholipid microbubbles for targeted tumor therapy: In-vivo characterization., J. Control. Release. 148 (2010) 368–72.

[23] C.-H. Fan, C.-Y. Ting, H.-J. Lin, C.-H. Wang, H.-L. Liu, T.-C. Yen, C.-K. Yeh, SPIO-conjugated, doxorubicin-loaded microbubbles for concurrent MRI and focused-ultrasound enhanced brain-tumor drug delivery., Biomaterials. 34 (2013) 3706–15.

[24] N. Sax, T. Kodama, Optimization of acoustic liposomes for improved in vitro and in

vivo stability., Pharm. Res. 30 (2013) 218–24.

[25] S. Ibsen, M. Benchimol, S. Esener, Fluorescent microscope system to monitor real-time interactions between focused ultrasound, echogenic drug delivery vehicles, and live cell membranes, Ultrasonics. 53 (2013) 178–184.

[26] S. Tinkov, G. Winter, C. Coester, R. Bekeredjian, New doxorubicin-loaded phospholipid microbubbles for targeted tumor therapy: Part I--Formulation development and in-vitro characterization., J. Control. Release. 143 (2010) 143–50.

[27] S.C. Tsinontides, P. Rajniak, D. Pham, W.A. Hunke, J. Placek, S.D. Reynolds, Freeze drying - Principles and practice for successful scale-up to manufacturing, Int. J. Pharm. 280 (2004) 1–16.

[28] F. Franks, Freeze-drying of bioproducts: Putting principles into practice, Eur. J. Pharm. Biopharm. 45 (1998) 221–229.

[29] C. Solis, F. Forsberg, M.A. Wheatley, Preserving enhancement in freeze-dried contrast agent ST68: Examination of excipients, Int. J. Pharm. 396 (2010) 30–38.

[30] P.C. Sontum, Physicochemical characteristics of Sonazoid, a new contrast agent for ultrasound imaging., Ultrasound Med. Biol. 34 (2008) 824–833.

[31] M. Schneider, SonoVue, a new ultrasound contrast agent, Eur. Radiol. 9 (1999) S347–S348.

[32] M. Schneider, M. Arditi, M.B. Barrau, J. Brochot, A. Broillet, R. Ventrone, F. Yan, BR1: A new ultrasonographic contrast agent based on sulfur hexafluoride-filled microbubbles., Invest. Radiol. 30 (1995) 451–7.

[33] W. Abdelwahed, G. Degobert, H. Fessi, Investigation of nanocapsules stabilization by amorphous excipients during freeze-drying and storage, Eur. J. Pharm. Biopharm. 63 (2006) 87–94.

[34] Y. Takakura, R.I. Mahato, M. Hashida, Extravasation of macromolecules, Adv. Drug Deliv. Rev. 34 (1998) 93–108.

[35] A.L. Klibanov, K. Maruyama, A.M. Beckerleg, V.P. Torchilin, L. Huang, Activity of amphipathic poly(ethylene glycol) 5000 to prolong the circulation time of liposomes depends on the liposome size and is unfavorable for immunoliposome binding to target., Biochim. Biophys. Acta. 1062 (1991) 142–148.

[36] W. Bin Cai, H.L. Yang, J. Zhang, J.K. Yin, Y.L. Yang, L.J. Yuan, L. Zhang, Y.Y. Duan, The optimized fabrication of nanobubbles as ultrasound contrast agents for tumor imaging., Sci. Rep. 5 (2015) 13725.

[37] P. Attard, The stability of nanobubbles, Eur. Phys. J. Spec. Top. (2013) 1–22.

[38] T.O. Matsunaga, P.S. Sheeran, S. Luois, J.E. Streeter, L.B. Mullin, B. Banerjee, P.A. Dayton, Phase-change nanoparticles using highly volatile perfluorocarbons: toward a

platform for extravascular ultrasound imaging, Theranostics. 2 (2012) 1185–1198.

[39] O. Couture, P.D. Bevan, E. Cherin, K. Cheung, P.N. Burns, F.S. Foster, Investigating perfluorohexane particles with high-frequency ultrasound, Ultrasound Med. Biol. 32 (2006) 73–82.

[40] N. Rapoport, K.-H. Nam, Droplet-to-bubble transition in phase-shift nanoemulsions for tumor chemotherapy., Int. J. Transp. Phenom. 12 (2011) 51–62.

[41] N. Reznik, R. Williams, P.N. Burns, Investigation of vaporized submicron perfluorocarbon droplets as an ultrasound contrast agent, Ultrasound Med. Biol. 37 (2011) 1271–1279.

[42] N. Rapoport, D.A. Christensen, A.M. Kennedy, K.-H. Nam, Cavitation properties of block copolymer stabilized phase-shift nanoemulsions used as drug carriers., Ultrasound Med. Biol. 36 (2010) 419–29.

[43] R. Williams, C. Wright, E. Cherin, N. Reznik, M. Lee, I. Gorelikov, F.S. Foster, N. Matsuura, P.N. Burns, Characterization of submicron phase-change perfluorocarbon droplets for extravascular ultrasound imaging of cancer, Ultrasound Med. Biol. 39 (2013) 475–489.

[44] K. Shiraishi, R. Endoh, H. Furuhata, M. Nishihara, R. Suzuki, K. Maruyama, Y. Oda, J.I. Jo, Y. Tabata, J. Yamamoto, M. Yokoyama, A facile preparation method of a PFC-containing nano-sized emulsion for theranostics of solid tumors, Int. J. Pharm. 421 (2011) 379–387.

[45] N.Y. Rapoport, A.M. Kennedy, J.E. Shea, C.L. Scaife, K.H. Nam, Controlled and targeted tumor chemotherapy by ultrasound-activated nanoemulsions/microbubbles, J. Control. Release. 138 (2009) 268–276.

[46] W.D. O'Brien, Ultrasound-biophysics mechanisms, Prog. Biophys. Mol. Biol. 93 (2007) 212–255.

[47] A. Pathak, S. Patnaik, K.C. Gupta, Recent trends in non-viral vector-mediated gene delivery, Biotechnol. J. 4 (2009) 1559–1572.

[48] M. Giacca, S. Zacchigna, Virus-mediated gene delivery for human gene therapy, J. Control. Release. 161 (2012) 377–388.

[49] S. Kawakami, Y. Higuchi, M. Hashida, Nonviral approaches for targeted delivery of plasmid DNA and oligonucleotide., J. Pharm. Sci. 97 (2008) 726–745.

[50] I. Lentacker, I. De Cock, R. Deckers, S.C. De Smedt, C.T.W. Moonen, Understanding ultrasound induced sonoporation: Definitions and underlying mechanisms, Adv. Drug Deliv. Rev. 72 (2014) 49–64.

[51] A. van Wamel, K. Kooiman, M. Harteveld, M. Emmer, F.J. ten Cate, M. Versluis, N. de Jong, Vibrating microbubbles poking individual cells: drug transfer into cells via

sonoporation., J. Control. Release. 112 (2006) 149–155.

[52] S.R. Sirsi, M.A. Borden, State-of-the-art materials for ultrasound-triggered drug delivery, Adv. Drug Deliv. Rev. 72 (2014) 3–14.

[53] J. Unga, M. Hashida, Ultrasound induced cancer immunotherapy, Adv. Drug Deliv. Rev. 72 (2014) 144–153.

[54] X. Wang, H.D. Liang, B. Dong, Q.L. Lu, M.J. Blomley, Gene transfer with microbubble ultrasound and plasmid DNA into skeletal muscle of mice: comparison between commercially available microbubble contrast agents, Radiology. 237 (2005) 224–229.

[55] Y. Negishi, D. Omata, H. Iijima, Y. Takabayashi, K. Suzuki, Y. Endo, R. Suzuki, K. Maruyama, M. Nomizu, Y. Aramaki, Enhanced laminin-derived peptide AG73-mediated liposomal gene transfer by bubble liposomes and ultrasound, Mol. Pharm. 7 (2010) 217–226.

[56] M. Barak, Y. Katz, Microbubbles: Pathophysiology and clinical implications, Chest. 128 (2005) 2918–2932.

[57] J. Alter, C.A. Sennoga, D.M. Lopes, R.J. Eckersley, D.J. Wells, Microbubble stability is a major determinant of the efficiency of ultrasound and microbubble mediated in vivo gene transfer., Ultrasound Med. Biol. 35 (2009) 976–84.

[58] R. Karshafian, P.D. Bevan, R. Williams, S. Samac, P.N. Burns, Sonoporation by ultrasound-activated microbubble contrast agents: effect of acoustic exposure parameters on cell membrane permeability and cell viability., Ultrasound Med. Biol. 35 (2009) 847–860.

[59] R. Suzuki, Y. Oda, N. Utoguchi, K. Maruyama, Progress in the development of ultrasound-mediated gene delivery systems utilizing nano- and microbubbles, J. Control. Release. 149 (2011) 36–41.

[60] S.B. Barnett, H.D. Rott, G.R. Ter Haar, M.C. Ziskin, K. Maeda, The sensitivity of biological tissue to ultrasound, Ultrasound Med. Biol. 23 (1997) 805–812..

[61] R. Suzuki, T. Takizawa, Y. Negishi, K. Hagisawa, K. Tanaka, K. Sawamura, N. Utoguchi, T. Nishioka, K. Maruyama, Gene delivery by combination of novel liposomal bubbles with perfluoropropane and ultrasound., J. Control. Release. 117 (2007) 130–136.

[62] K. Sarkar, A. Katiyar, P. Jain, Growth and dissolution of an encapsulated contrast microbubble: Effects of encapsulation permeability, Ultrasound Med. Biol. 35 (2009) 1385–1396.

[63] J. Kwan, M. Borden, Microbubble shell break-up and collapse during gas exchange, in: Proc. - IEEE Ultrason. Symp., 2010: pp. 897–899.

[64] C.D. Walkey, W.C.W. Chan, Cancer theranostics, 2014.

[65] S. Svenson, Theranostics: Are we there yet?, Mol. Pharm. 10 (2013) 848–856.

[66] R. Lencioni, F. Piscaglia, L. Bolondi, Contrast-enhanced ultrasound in the diagnosis of hepatocellular carcinoma, J. Hepatol. 48 (2008) 848–857.

[67] M.A. Pysz, I. Guracar, K. Foygel, L. Tian, J.K. Willmann, Quantitative assessment of tumor angiogenesis using real-time motion-compensated contrast-enhanced ultrasound imaging, Angiogenesis. 15 (2012) 433–442.

[68] S.R. Sirsi, M.L. Flexman, F. Vlachos, J. Huang, S.L. Hernandez, H.K. Kim, T.B. Johung, J.W. Gander, A.R. Reichstein, B.S. Lampl, A. Wang, A.H. Hielscher, J.J. Kandel, D.J. Yamashiro, M.A. Borden, Contrast ultrasound imaging for identification of early responder tumor models to anti-angiogenic therapy, Ultrasound Med. Biol. 38 (2012) 1019–1029.

[69] K. Ogawara, K. Un, K. Tanaka, K. Higaki, T. Kimura, In vivo anti-tumor effect of PEG liposomal doxorubicin (DOX) in DOX-resistant tumor-bearing mice: Involvement of cytotoxic effect on vascular endothelial cells., J. Control. Release. 133 (2009) 4–10.

[70] Y. Negishi, N. Hamano, Y. Tsunoda, Y. Oda, B. Choijamts, Y. Endo-Takahashi, D. Omata, R. Suzuki, K. Maruyama, M. Nomizu, M. Emoto, Y. Aramaki, AG73-modified Bubble liposomes for targeted ultrasound imaging of tumor neovasculature, Biomaterials. 34 (2013) 501–507.

[71] X. Dai, Z. Yue, M.E. Eccleston, J. Swartling, N.K.H. Slater, C.F. Kaminski, Fluorescence intensity and lifetime imaging of free and micellar-encapsulated doxorubicin in living cells., Nanomedicine. 4 (2008) 49–56.

[72] M.J. McKeage, B.C. Baguley, Disrupting established tumor blood vessels: An emerging therapeutic strategy for cancer, Cancer. 116 (2010) 1859–1871.

[73] R.J. Price, D.M. Skyba, S. Kaul, T.C. Skalak, Delivery of colloidal particles and red blood cells to tissue through microvessel ruptures created by targeted microbubble destruction with ultrasound., Circulation. 98 (1998) 1264–1267.

[74] Y. Matsumura, H. Maeda, A new concept for macromolecular therapeutics in cancer chemotherapy: Mechanism of tumoritropic accumulation of proteins and the antitumor agent smancs, Cancer Res. 46 (1986) 6387–6392.

[75] J. Fang, H. Nakamura, H. Maeda, The EPR effect: Unique features of tumor blood vessels for drug delivery, factors involved, and limitations and augmentation of the effect, Adv. Drug Deliv. Rev. 63 (2011) 136–151.

[76] H. Maeda, J. Wu, T. Sawa, Y. Matsumura, K. Hori, Tumor vascular permeability and the EPR effect in macromolecular therapeutics: A review, J. Control. Release. 65

(2000) 271–284.

[77] N.D. James, R.J. Coker, D. Tomlinson, J.R.W. Harris, M. Gompels, A.J. Pinching, J.S.W. Stewart, Liposomal doxorubicin (Doxil): An effective new treatment for Kaposi's sarcoma in AIDS, Clin. Oncol. 6 (1994) 294–296.

[78] Y. Barenholz, Doxil?? - The first FDA-approved nano-drug: Lessons learned, J. Control. Release. 160 (2012) 117–134.

[79] E. Quaia, Microbubble ultrasound contrast agents: An update, Eur. Radiol. 17 (2007) 1995–2008.

[80] J. Ruiz-Cabello, B.P. Barnett, P.A. Bottomley, J.W.M. Bulte, Fluorine (19F) MRS and MRI in biomedicine, NMR Biomed. 24 (2011) 114–129.

[81] X. Fan, J.N. River, A.S. Muresan, C. Popescu, M. Zamora, R.M. Culp, G.S. Karczmar, MRI of perfluorocarbon emulsion kinetics in rodent mammary tumours., Phys. Med. Biol. 51 (2006) 211–20.

[82] T.M. Allen, L.G. Cleland, Serum-induced leakage of liposome contents, BBA - Biomembr. 597 (1980) 418–426.

[83] P.S. Sheeran, P. a Dayton, Improving the performance of phase-change perfluorocarbon droplets for medical ultrasonography: Current progress, challenges, and prospects., Scientifica (Cairo). 2014 (2014) 579684.

[84] N. Rapoport, K.H. Nam, R. Gupta, Z. Gao, P. Mohan, A. Payne, N. Todd, X. Liu, T. Kim, J. Shea, C. Scaife, D.L. Parker, E.K. Jeong, A.M. Kennedy, Ultrasound-mediated tumor imaging and nanotherapy using drug loaded, block copolymer stabilized perfluorocarbon nanoemulsions, J. Control. Release. 153 (2011) 4–15.

[85] D. Thakkar, R. Gupta, K. Monson, N. Rapoport, Effect of ultrasound on the permeability of vascular wall to nano-emulsion droplets, Ultrasound Med. Biol. 39 (2013) 1804–1811.

[86] K. Shiraishi, R. Endoh, H. Furuhata, M. Nishihara, R. Suzuki, K. Maruyama, Y. Oda, J. Jo, Y. Tabata, J. Yamamoto, M. Yokoyama, A facile preparation method of a PFC-containing nano-sized emulsion for theranostics of solid tumors., Int. J. Pharm. 421 (2011) 379–87.

[87] M.L. Fabiilli, M.R. Piert, R.A. Koeppe, P.S. Sherman, C.A. Quesada, O.D. Kripfgans, Assessment of the biodistribution of an [18F]FDG-loaded perfluorocarbon double emulsion using dynamic micro-PET in rats, Contrast Media Mol. Imaging. 8 (2013) 366–374.

[88] P.K. Bentley, L. Johnson, Uptake of concentrated perfluorocarbon emulsions into rat lymphoid tissues, (1993) 182–185.

[89] B. Canaud, P. Aljama, C. Tielemans, V. Gasparovic, A. Gutierrez, F. Locatelli, Pathochemical toxicity of perfluorocarbon-5070, a liquid test performance fluid previously used in dialyzer manufacturing, confirmed in animal experiment., J. Am. Soc. Nephrol. 16 (2005) 1819–1823.

[90] M. Zhang, M.L. Fabiilli, K.J. Haworth, J.B. Fowlkes, O.D. Kripfgans, W.W. Roberts, K.A. Ives, P.L. Carson, Initial investigation of acoustic droplet vaporization for occlusion in canine kidney, Ultrasound Med. Biol. 36 (2010) 1691–1703.

[91] J. van der Zee, Heating the patient: A promising approach?, Ann. Oncol. 13 (2002) 1173–1184.

[92] G. Ter Haar, C. Coussios, High intensity focused ultrasound: Physical principles and devices, Int. J. Hyperth. 23 (2007) 89–104.

[93] M. Aujla, HIFU for prostate cancer, Nat. Rev. Clin. Oncol. 6 (2009) 497–497.

[94] O. Al-Bataineh, J. Jenne, P. Huber, Clinical and future applications of high intensity focused ultrasound in cancer, Cancer Treat. Rev. 38 (2012) 346–353.

[95] G. Malietzis, L. Monzon, J. Hand, H. Wasan, E. Leen, M. Abel, A. Muhammad, P. Price, P. Abel, High-intensity focused ultrasound: Advances in technology and experimental trials support enhanced utility of focused ultrasound surgery in oncology, Br. J. Radiol. 86 (2013) 1024.

[96] S. Umemura, S. Yoshizawa, R. Takagi, Y. Inaba, J. Yasuda, Enhancement of focused ultrasound treatment by acoustically generated microbubbles, Jpn. J. Appl. Phys. 52 (2013) 07HA02.

[97] T. Yu, G. Wang, K. Hu, P. Ma, J. Bai, Z. Wang, A microbubble agent improves the therapeutic efficiency of high intensity focused ultrasound: A rabbit kidney study, Urol. Res. 32 (2004) 14–19.

[98] K. Kajiyama, K. Yoshinaka, S. Takagi, Y. Matsumotod, Micro-bubble enhanced HIFU, in: Phys. Procedia. 3 (2010) 305–314.

[99] C.H. Farny, R. Glynn Holt, R.A. Roy, The correlation between bubble-enhanced HIFU heating and cavitation power, IEEE Trans. Biomed. Eng. 57 (2010) 175–184.

[100] P. Zhang, T. Porter, An in vitro study of a phase-shift nanoemulsion: A potential nucleation agent for bubble-enhanced HIFU tumor ablation, Ultrasound Med. Biol. 36 (2010) 1856–1866.

[101] M. Hashida, S. Kawakami, F. Yamashita, Lipid carrier systems for targeted drug and gene delivery, Chem. Pharm. Bull. (Tokyo). 53 (2005) 871–880.

[102] M. Hashida, Y. Takahashi, S. Muranishi, H. Sezaki, An application of water-in-oil and gelatin-microsphere-in-oil emulsions to specific delivery of anticancer agent into stomach lymphatics, J. Pharmacokinet. Biopharm. 5 (1977) 241–255.

[103] T. Nomura, N. Koreeda, F. Yamashita, Y. Takakura, M. Hashida, Effect of particle size and charge on the disposition of lipid carriers after intratumoral injection into tissue-isolated tumors, Pharm. Res. 15 (1998) 128–132.

[104] S.T. Kang, Y.C. Lin, C.K. Yeh, Mechanical bioeffects of acoustic droplet vaporization in vessel-mimicking phantoms, Ultrason. Sonochem. 21 (2014) 1866–1874.

[105] Y. Yuksel Durmaz, E. Vlaisavljevich, Z. Xu, M. Elsayed, Development of nanodroplets for histotripsy-mediated cell ablation, Mol. Pharm. 11 (2014)

[106] E. Vlaisavljevich, Y.Y. Durmaz, A. Maxwell, M. ElSayed, Z. Xu, Nanodroplet-mediated histotripsy for image-guided targeted ultrasound cell ablation, Theranostics. 3 (2013) 851–864.

[107] H.-L. Liu, H.-Y. Hsieh, L.-A. Lu, C.-W. Kang, M.-F. Wu, C.-Y. Lin, Low-pressure pulsed focused ultrasound with microbubbles promotes an anticancer immunological response., J. Transl. Med. 10 (2012) 221.

[108] R. Suzuki, Y. Oda, D. Omata, N. Nishiie, R. Koshima, Y. Shiono, Y. Sawaguchi, J. Unga, T. Naoi, Y. Negishi, S. Kawakami, M. Hashida, K. Maruyama, Tumor growth suppression by the combination of nanobubbles and ultrasound, Cancer Sci. 107 (2016) 217–223.